

The optimal design for photovoltaic power plants on sites with a general slope

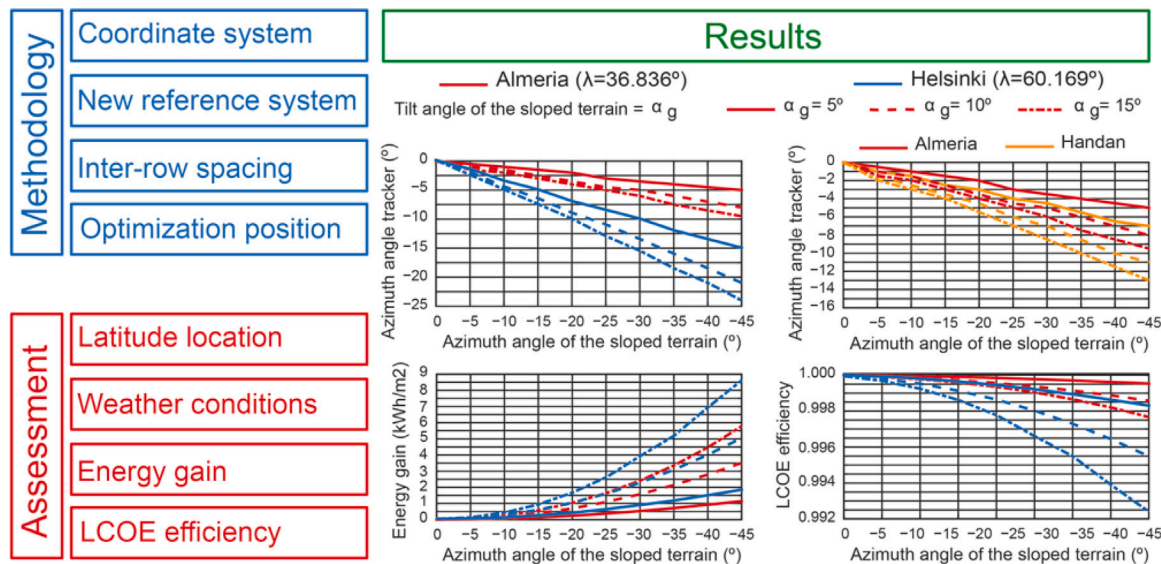
A. Barbón ^a, J. Aparicio-Bermejo ^b, L. Bayón ^c,* , P. Fortuny Ayuso ^c

^a Department of Electrical Engineering, University of Oviedo, Spain

^b Business Development Iberia Northwest Area, Enel Green Power, 28014 Madrid, Spain

^c Department of Mathematics, University of Oviedo, Spain

GRAPHICAL ABSTRACT



ARTICLE INFO

Keywords:

Horizontal single-axis trackers

Sloping terrain

Optimising the deployment of solar trackers

ABSTRACT

Some of the characteristics of sloping terrain may favour the development of *PV* power plant projects. However, the deployment of the solar trackers must be optimised in order to avoid significant production losses due to the azimuth angle and the angle of inclination of the terrain. Such optimisation leads to a complex problem, involving 14 variables. The optimal choice of azimuth angle (γ) and tilt angle (α) of a solar tracker for terrain defined by a given azimuth angle (γ_g) and tilt angle (α_g) is by no means trivial. This is the main objective of this paper. Moreover, an optimal *PV* power plant design requires inter-row spacing that avoid shading between adjacent *PV* modules in addition to determining the ideal operating periods. Numerical values are presented for 10 locations in the Northern Hemisphere, with terrain azimuth angles between 0° and $\pm 45^\circ$, and terrain tilt angles between 0° and 15° . The following main conclusions can be highlighted: (i) The robustness of the derived equations was proven by validating them from three points of view: numerical validation, validation using PVsyst and Mathematica software and experimental validation; (ii) The azimuth angle of the *PV* system located at high latitudes is strongly affected by the azimuth angle of the terrain. In contrast, at low latitude locations, the azimuth angle of the terrain has very little influence;

* Corresponding author.

E-mail address: bayon@uniovi.es (L. Bayón).

(iii) The azimuth angle of the *PV* system, if the latitude of the site is kept constant, is affected by the weather conditions throughout the year; (iv) Regarding energy gain (*EG*), for *PV* system site latitudes between 6° and 19°, the optimal deployment does not achieve significantly better results than deploying the *PV* system in a southerly direction. In contrast, if this comparison is made at locations with latitudes above 19°, the *EG* is significant: (a) The higher the latitude, the higher the *EG*; (b) The higher the γ_g , the higher the *EG*; and (c) The higher the α_g , the higher the *EG*. Using Almeria as a baseline for comparison purposes, with $\alpha_g = 5^\circ$, $\gamma_g = 20^\circ$ and $EG = 240$ (Wh/m²), the *EG* is 390 (Wh/m²) in Helsinki with the same parameters. When $\gamma_g = 30^\circ$ in Almeria, the *EG* is 530 (Wh/m²). When $\alpha_g = 15^\circ$ in Almeria, the *EG* is 1030 (Wh/m²). (v) Regarding *LCOE* efficiency, for latitudes between 6° and 19°, the values obtained are similar to those provided by the southward deployment of solar trackers. For latitudes higher than 19° the following hold: (a) The higher the latitude, the higher the *LCOE* of the optimal deployment. (b) The higher the azimuthal terrain angle, the higher the *LCOE*, and (c) The higher the terrain tilt angle, the higher the *LCOE*. Therefore, it can be concluded that the deployment of *PV* systems at high latitudes is strongly affected by the azimuth angle of the terrain.

1. Introduction

The signatories to the Paris Agreement aim to curb CO₂ emissions and ensure sustainable development [1]. In this respect, the European Union (EU) has the ambitious goal of becoming climate neutral by 2050 [2], which requires the decarbonisation of energy systems. To comply with the Paris agreements, it has been estimated that the energy capacity of renewable energies must grow by more than 1000 (GW/year) by 2030 [3]. In 2022, 83% (300 (GW)) of new electricity generation capacity came from renewable energies [3], compared to 17% from fossil fuels and nuclear power. Therefore, the share of renewable energies should grow substantially. Solar and wind energy are expected to play a dominant role in achieving this goal [4]. An IEA report forecasts a significant increase in the use of photovoltaic technologies [5] because of their contribution to the ongoing reduction in the levelized cost of energy (*LCOE*), among other aspects. The evolution of the installed capacity of *PV* systems compared to 2012 is shown in Fig. 1 [6]. This technology has grown by 280% in five years and by 910% in ten years. The trend is very positive for this technology.

Three *PV* mounting system configurations are typically used in large-scale *PV* power plants [7]: dual-axis trackers, single-axis trackers, and annual fixed tilt angle. Dual-axis trackers are characterised by two degrees of freedom in their movement to ensure that the maximum possible beam irradiance is received [8]. This advantage is the cause of their major disadvantages, sensitivity to wind loads and high operating and maintenance costs [9]. Single-axis trackers are characterised by a degree of freedom of movement. This tracker is divided into three configurations: (i) horizontal single-axis tracker, (ii) vertical single-axis tracker and (iii) tilted single-axis tracker. The most commonly used is the first configuration. This configuration is characterised by the fact that its axis of rotation is horizontal with respect to the ground, and therefore the *PV* modules are oriented parallel to the axis of rotation. In turn, this horizontal axis can be oriented in two configurations: East–West (*E – W*) or North–South (*N – S*). With the *N – S* (*E – W*) configuration, the modules follow the Sun in the *E – W* (*N – S*) tracking direction. The *N – S* configuration produces the most energy [8]; therefore, they are the most commonly used single-axis trackers (hereinafter referred to as horizontal single-axis trackers). This type of tracker, however, produces less energy than a dual-axis tracker [8], yet is less sensitive to wind loads and leads to lower operating and maintenance costs [9]. Finally, the *PV* mounting system configuration with an annual fixed tilt angle produces the least energy of the three configurations [8], in addition to generating the lowest operating and maintenance costs [9].

PV power plant developers have historically based their choice of a *PV* mounting system on the highest system reliability, durability and maintenance efficiency [10]. Due to their longer lifespan when compared with dual-axis trackers, horizontal single-axis trackers outperform the former in terms of reliability [11]. They also outperform dual-axis trackers because of their lower initial and maintenance

costs [9]. For these reasons, the use of horizontal single-axis trackers is prioritised [10]. According to a report by [12], horizontal single-axis trackers have a market share of more than 95%. The most important reasons: they are inexpensive, easy to install and operate at a minimal cost. These reasons were the motivation in this study to focus on this solar tracker configuration. The economic data available support this choice. According to a research report published by [10], the worldwide global solar tracker market size was valued at USD 3.2 billion in 2022, and is expected to reach USD 7.2 billion by 2033.

The first large-scale *PV* power plants have been installed on flat land with minimal variation in terrain topography. The cost reduction at these locations is obvious. Several studies are available to facilitate the simulation and design of such projects [13,14]. However, considering the remarkable growth of *PV* energy, projects are now being developed in areas where the topography is irregular. Some characteristics of areas with irregular topography can favour the development of *PV* power plant projects, such as:

- (i) An increase in available arable land. Land with irregular topography is not suitable for use as arable land. The need for large areas of flat land for the implementation of a *PV* power plant has been identified as one of the main negative impacts on agriculture [15]. The land available for agricultural activities has in fact decreased due to *PV* power plant projects [16]. According to a report by the Food and Agriculture Organisation [17], approximately 33% of the world's land surface is used for agricultural purposes, with arable land accounting for 33% of this agricultural land. Considering that only 10% of the world's land surface is arable land, decreasing this percentage by installing *PV* power plants is a decision that could lead to a rise in food shortages. Therefore, 66% of agricultural land (forests, mountains and inland water bodies) can be put to other uses, such as the installation of *PV* power plants, in order to free up arable land. Inland water bodies are already being used for the installation of floating *PV* power plants [18].
- (ii) An increase in annual incident solar irradiation. A study conducted by [19] at 10 locations in the northern hemisphere, with latitudes ranging from 6° to 60°, showed that the average annual incident energy gain with horizontal single-axis trackers installed on land with irregular topography reached values of more than 13.5% compared to their installation on flat land.
- (iii) The cost of land with irregular topography. The average price of arable land in the European Union (EU) was 10,578 (€/ha) in 2022 [20]. Obviously, the average price of arable land varies significantly from region to region. On the other hand, in the same year, the average price of renting arable land and/or permanent pasture was 199 (€/ha) [20]. There are also notable differences from one Member State to another. The physical characteristics of any given land surface, i.e. the topography, determine the value of the land. The cost of land with uneven topography is cheaper. If the slope of the land is higher than 15%, the price of the land decreases significantly [21].

Nomenclature

A_{TPV}	Total photovoltaic modules area (m ²)
d_{\min}	Minimum distance $E - W$ between two adjacent mounting systems (m)
d_r	Annual degradation rate
d_{st}	Standard distance $E - W$ between two adjacent mounting systems (m)
E_a	Total incident energy on the PV field (Wh)
EG	Energy Gain (kWh/m ²)
e_l	Distance $N - S$ between two adjacent mounting systems (m)
e_t	Pitch (m)
H_a	Annual incident solar irradiation on the PV field (Wh/m ²)
H_t	Daily incident solar irradiation on the PV field (Wh/m ²)
k_d	Cloudiness index (dimensionless)
I_{bh}	Beam irradiance on a horizontal surface (W/m ²)
I_{dh}	Diffuse irradiance on a horizontal surface (W/m ²)
I_{gh}	Global irradiance on a horizontal terrain (W/m ²)
I_t	Total incident solar irradiance on the PV field (W/m ²)
L	Length of the solar tracker (m)
L_{PV}	Length of the photovoltaic modules (m)
$LCOE$	Levelised cost of electricity (€/kWh)
efficiency	Ratio between the $LCOE$ s deployment solar trackers
N	Lifetime of the project (years)
$NOCT$	Normal Operating Cell Temperature (°C)
N_{PV}	Number of photovoltaic modules
n	Ordinal of the day (day)
q_{PV}	Load due to the weight of the PV modules (kN/m ²)
r	Discount rate for $i - th$ year
SED	Energy difference due to the software used (%)
T	Solar time (h)
T_R	Sunrise solar time (h)
T_S	Sunset solar time (h)
T_{b1}	End of the backtracking mode (h)
T_{b2}	Start of the backtracking mode (h)
$T_{\beta 1}$	Start of the normal tracking mode (h)
$T_{\beta 2}$	End of the normal tracking mode (h)
T_a	Ambient temperature (°C)
T_c	PV cell temperature (°C)
T_{ref}	Reference temperature (°C)
W	Width of the solar tracker (m)
W_{PV}	Width of the photovoltaic modules (m)
α	Tilt angle of solar tracker (°)
α_g	Tilt angle of the terrain (°)
β	Tilt angle of photovoltaic module (°)
β_B	Backtracking angle (°)
β_c	Tilt angle between rows of trackers (°)
β_{\max}	Limited range of motion angle (°)
β_{st}	Standard tilt angle of photovoltaic module (°)
γ	Azimuth angle of solar tracker (°)
γ_g	Azimuth angle of the sloped surface (°)

δ	Solar declination (°)
η_e	Electrical efficiency (dimensionless)
η_{ref}	Reference electrical efficiency (dimensionless)
θ	Incidence angle (°)
θ_t	Transversal angle (°)
θ_{tb}	Backtracking angle (°)
θ_{tst}	Standard transversal angle (°)
θ_z	Zenith angle of the Sun (°)
λ	Latitude angle (°)
ρ_g	Ground reflectance (dimensionless)
ω	Hour angle (°)

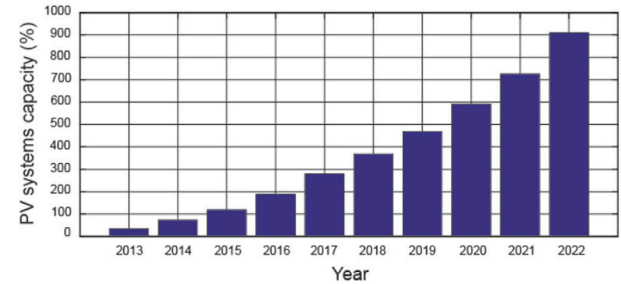


Fig. 1. Global PV systems installed capacity.

1.1. Review of the literature

Nowadays, land levelling for the installation of photovoltaic power plants is discarded due to its high cost [7]. Despite studies optimising the levelling of the terrain [22], it is always cheaper to adapt to the conditions of the terrain [7]. This requires the development of an optimisation methodology for solar trackers on sloping terrain with variable orientation.

The operating modes of an horizontal single-axis tracker are defined by the position of the Sun, the shadows cast by the PV modules and the rotational constraints. There are three different possibilities [14]: (i) backtracking mode, (ii) static mode, and (iii) normal tracking mode.

During the operation mode of a horizontal single-axis tracker, shading between the PV modules should be avoided, especially at periods of low solar elevation (sunrise and sunset), when some of the PV modules may cast shadows on others. This gives rise to the backtracking mode, during which a specific algorithm determines the tilt angle of the PV modules which avoids casting shadows on other modules while maximising the solar irradiance.

Solar trackers have a limited rotation range (influenced in part by the wind and snow loads at the location of the power plant), which is usually $\beta_{\max} = \pm 60^\circ$ [7]. This creates a constraint which prevents, at some times, the optimal theoretical orientation of the panels, and forces them to remain static at a specific tilt angle β_{\max} . This mode of operation is referred to as static.

During the normal tracking operation, the algorithm places the PV modules in the position that maximises the cosine of the solar incidence angle [23] in order to maximise the incident beam solar irradiance on the PV modules.

When designing a single-axis tracker control system, the equations that define the operating modes must be known [14]: (i) backtracking mode, (ii) static mode, and (iii) normal tracking mode. The precise times when each of these operating modes begins and ends must also be known. The power generated by PV modules depends on the exact knowledge of these parameters. However, only a few studies related to these trackers take into account all three modes of operation. The variations in topography with respect to flat land means that equations

Table 1
Input variables involved in the design of a PV power plant.

Identifier	Variable
Id_1	Location: latitude (λ), longitude (l), altitude (A), cloudiness index (k_d)
Id_2	Azimuth angle of the generic sloped surface (γ_g)
Id_3	Tilt angle of the terrain (α_g)
Id_4	Azimuth angle of solar tracker (γ)
Id_5	Tilt angle of solar tracker (α)
Id_6	Configuration of PV modules (1V, 2V)
Id_7	PV module dimensions (L_{PV} , W_{PV})
Id_8	Limited range of motion angle (β_{max})
Id_9	Min. dist. between rows of trackers to allow maintenance (d_{min})
Id_{10}	Transversal solar angle for avoiding shading in Standard (θ_{st})
Id_{11}	Inter-row spacing (e_r)
Id_{12}	Periods of operation in normal tracking mode (T_{β_1} , T_{β_2})
Id_{13}	Periods of operation in backtracking mode (T_{R_1} , T_{b_1}), (T_{b_2} , T_S)
Id_{14}	Periods of operation in static mode (T_{β_1} , T_{β_2}), (T_{β_2} , T_{b_2})

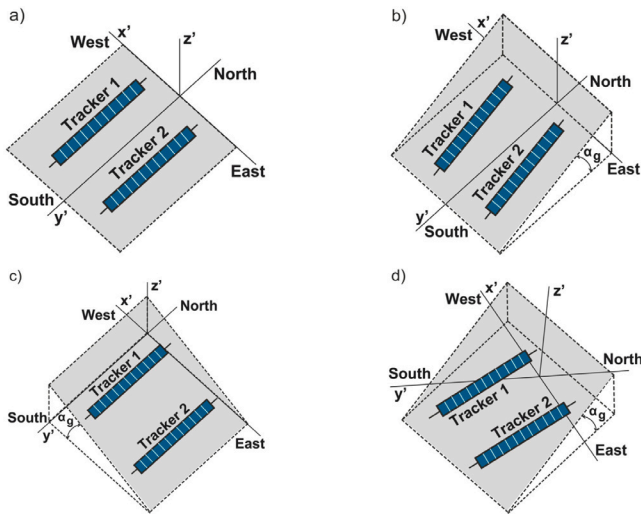


Fig. 2. Possible orientations and tilt angles of the land.

designed for flat surfaces [14] are not applicable in these cases. Designing of new equations that adapt to sloped land will be one of the objectives of this paper.

Very few studies have focused on the design of PV power plants deployed on terrain oriented in any direction and on any slope [24]. This is a complex problem due to the number of design variables involved. There are 14 input variables involved in the design of a PV power plant deployed on terrain oriented in any direction and any inclination.

Section 2 details each of these variables, which are presented in Table 1. The first three identifiers are determined by the location chosen for the PV power plant. The remaining identifiers affect plant design and an optimal choice thereof affects the energy generated by a PV power plant and, therefore, its profitability. Thus, choosing these identifiers well is necessary when seeking to maximise the annual incident energy in the PV field. Fig. 2 shows the possible orientations and tilt angles of the land used for the layout of horizontal single-axis trackers. We proceed to survey the studies related to each configuration.

Fig. 2a shows the layout of horizontal single-axis trackers on a horizontal surface.

- (i) Casares et al. [25] presented a study of the layout of a PV plant on a horizontal surface (variable Id_2 and Id_3 not considered) in which the backtracking mode and the normal tracking mode are taken into account. The equations for these operating modes are presented, however the limited rotation range of the solar tracker is not taken into account (variable Id_8 not considered).

The equations presented cannot be used in the case under study.

- (ii) This layout has also been studied in a paper by [14], which presented an optimisation methodology that takes into account design variables such as irregular land shape, the size and configuration of the PV mounting system, row spacing and the three operating periods. Equations for calculating the optimal row spacing and operating periods were presented, and a packing algorithm was used to optimise the number of solar trackers for a given available area. Nonetheless, variable Id_2 and Id_3 were not considered given that the layout of the horizontal single-axis trackers is on a horizontal surface. The only variables considered were Id_6 , Id_7 , Id_8 , Id_9 , Id_{10} , and Id_{11} . Due to the slope of the terrain, the equations presented cannot be used in this study.

Fig. 2b shows the layout of several horizontal single-axis trackers fulfilling the following conditions: (i) south-facing sloping terrain, and (ii) south-facing trackers. This layout is a particular case of the study presented here.

- (iii) The equations governing the motion of a horizontal single-axis tracker deployed on sloped terrain are deduced and experimentally verified in this work [19]. Although variable Id_2 is considered in this paper, it is considered to be constant ($\gamma_g = 0^\circ$). Instead, if you consider the variables Id_3 , Id_6 , Id_7 , Id_8 , Id_9 , Id_{10} , and Id_{11} . Since the sloped surface can feature any azimuthal angle, the equations presented cannot be used in this study.

- (iv) Huang et al. [26] determine the optimal tilt angle of solar trackers based on a spatial projection model and a dynamic shadow evaluation method. As it covers a single location (Ningxia, China), weather conditions are not studied. It does not take into account the indicators (Id_2 , Id_4 , Id_5 , Id_6 , and Id_7).

- (v) Pierce et al. [27] model the backtracking mode of operation in the deployment of solar trackers on sloping terrain. It does not take into account the indicators (Id_2 , Id_6 , Id_7 , Id_8 , Id_9 , Id_{10} , and Id_{11}).

- (vi) Bruno et al. [28] presented the equations for two strategies aimed at controlling the angle of rotation of PV modules around a horizontal tilted axis. Said paper does not consider most of the variables raised in this study (Id_2 , Id_3 , Id_6 , Id_7 , Id_8 , Id_9 , Id_{10} , and Id_{11}). Therefore, the equations submitted cannot be used in this study.

Fig. 2c shows the layout of several horizontal single-axis trackers fulfilling the following conditions: (i) east-facing sloping terrain, and (ii) south-facing trackers. This layout is a particular case of the study presented here.

- (vii) Anderson [29] presents the equations for three backtracking strategies as a function of the array geometry and the steepness of the cross-axis grade. Said paper does not consider most of the variables raised in this study (Id_2 , Id_6 , Id_7 , Id_8 , Id_9 , Id_{10} , and Id_{11}). As it is a particular case of the study presented here and does not take into account fundamental identifiers in the design of a PV power plant, the equations presented cannot be used in this study.

Fig. 2d shows the layout of several horizontal single-axis trackers fulfilling the following conditions: (i) sloping terrain oriented in any direction, and (ii) trackers oriented in the optimal direction and tilt angle (which must be determined in order to maximise the incident solar irradiance on the PV field).

- (viii) Lorenzo et al. [30] presents the equations for the position of the Sun, but does not present the equations needed to calculate the tracker operating periods nor does it take into account indicators (Id_2 , Id_3 , Id_6 , Id_7 , Id_8 , Id_9 , Id_{10} , and Id_{11}) which are fundamental to the design of a PV power plant.

- (ix) Anderson and Mikofski [31] present the equations for the true tracking angle, the backtracking angle, and the shaded fraction of horizontal-axis solar trackers deployed on slopes of arbitrary orientation. It does not take into account the indicators (Id_4 , Id_5 , Id_6 , Id_7 , Id_8 , Id_9 , Id_{10} , and Id_{11}) which are essential to the design of a *PV* power plant. In addition, it does not calculate energies. It only calculates tracker positions with the aforementioned limitations. Furthermore, it does not optimise the tracker position for sloped land.
- (x) Gómez-Uceda et al. [24] presented a study on the optimal orientation of horizontal single-axis trackers over sloping terrain with a variable orientation. One limitation of said study is that it focused only on one location in southern Spain. Moreover, the study does not present a layout that is optimal for planning or the influence of weather conditions. The results obtained in said study indicated that for non-south-facing terrain, the azimuth of the axis of rotation of horizontal single-axis trackers should be non-zero. It determined the incident energy in the *PV* field and optimises the tracker position for the tilted land using Lagrange multipliers. It does not take into account the indicators (Id_1 , Id_6 , Id_7 , Id_8 , Id_9 , Id_{10} , and Id_{11}) essential for the design of a *PV* power plant.
- (xi) Ledesma et al. [32] study the optimal orientation of horizontal single-axis trackers on sloping terrain with a variable orientation. The study is focused on one single location in central Spain, and therefore does not analyse the influence of meteorological conditions. None of the essential indicators (Id_1 , Id_6 , Id_7 , Id_9 , and Id_{10}) are covered in it.
- (xii) López [33] present an analysis of the tilt angle and orientation of solar trackers in a real *PV* power plant in central Spain. Again, as it deals with a single location, It does not take into account the weather. Also, indicators (Id_1 , Id_2 , Id_3 , and Id_6) are not covered.
- (xiii) Aronescu and Appelbaum [34] study fixed tilt angle mounting systems deployed in any azimuth in horizontal or inclined plane. Obviously, the equations derived cannot be applied to solar trackers.
- (xiv) Anderson and Jensen [35] generalise the equations for horizontal single-axis trackers deployed on cross-slope terrain. This study does not take into account the indicators (Id_2 , Id_6 , Id_7 , Id_8 , Id_9 , Id_{10} , and Id_{11}).

Decision-making in *PV* projects is associated with the analysis of the economic benefits associated with the deployment of solar trackers. We provide a cost analysis in ANNEX B, which none of the papers above do.

The above literature review indicates that studies that take into account the necessary indicators for the optimal design of a *PV* power plant with horizontal single-axis trackers deployed on tilted land and oriented in any direction are incomplete. Therefore, research is needed that takes into account all indicators of an optimal design for a *PV* power plant deployed on an inclined surface oriented in any direction, as the equations needed to apply them in practice are not currently available to *PV* power plant design professionals.

1.2. Scientific contributions

Based on the limitations and shortcomings of the works above, we have identified objectives and proposed a methodology to address the research gaps found in previous studies.

The proposed methodology focuses on determining three factors: (i) the equations defining the correct motion of the tracker, (ii) its operating periods, and (iii) the optimal layout on a sloping terrain with arbitrary orientation. This methodology uses the following steps: (i) find the optimal coordinate system, (ii) find the relationship between the angles of the terrain (α_g and γ_g) and those of the tracker (α and γ), (iii) transform the reference system S' into the system S'' , (iv) establish

the inter-row spacing, (v) determine the three operating periods and the motion of the tracker, (vi) optimise the position of the trackers, and (vii) validation. That is, we have developed equations that optimise the azimuthal angle and tilt angle of the solar tracker as a function of tilted land orientation. Unlike all previous work reviewed, this study takes into account all the indicators necessary for the design of a photovoltaic plant. In addition, a detailed economic study is presented.

Various commercial software programs (PVsyst [36], SolarFarmer [37], RETScreen [38], etc.) can be used to determine the power output of a *PV* power plant with horizontal single-axis trackers oriented in any direction and with any slope. However, the layout of the solar trackers must be entered in these programs as the main data. Such process is highly complicated given the large number of identifiers. The work presented here facilitates this task by optimising the layout of the solar trackers on the available terrain. Specifically, the main contributions of this study are as follows:

- (i) Determining the equations for each of the operating modes: tracking mode, static mode and normal tracking mode, in order to maximise the electrical energy production.
- (ii) Optimising the position of horizontal single-axis trackers (tilt angle (Id_4) and the azimuth angle (Id_5)) to maximise the annual incident solar irradiance on the *PV* field. The layout of the solar tracker must be entered in specialised software (PVsyst [36], SolarFarmer [37], RETScreen [38], etc.) as the main data in order to calculate the photovoltaic systems.
- (iii) Analysing the influence of latitude on the optimisation of a solar tracker layout.
- (iv) Analysing the influence of local weather conditions on the optimisation of a solar tracker layout.
- (v) Analysing the energy gain from optimising the layout of a solar tracker.
- (vi) Analysing the economic benefit of optimal solar tracker deployment.

In summary, there are two issues to be solved: (i) the optimal choice of a solar tracker layout for a sloping terrain oriented in any direction, and (ii) the determination of the equations that define the correct operation of the solar tracker movement.

The remainder of the paper is organised as follows: Section 2 presents the detailed formulation of the problem. Section 3 shows the proposed methodology, which consists of the following steps: (i) co-ordinating the system deduction, (ii) the deduction of the relationship between the angles of the sloping terrain and the angles of the solar tracker, (iii) the transformation of the reference system S' into the system S'' , (iv) the inter-row spacing design, (v) the determination of operating periods and the motion of the solar tracker, (vi) the optimisation of the position of the solar trackers, (vii) the validation of the model, and (viii) the limitations of the study. Section 4 provides the evaluation indicators. Section 5 presents the results obtained at ten locations in the northern hemisphere. Finally, the main conclusions of this work are drawn in Section 6.

2. Problem statement

The annual energy incident on *PV* modules is one of the key data when deciding on the installation of a *PV* power plant at a given location. It is even more important in this case given that, the terrain may be oriented in any direction and at any inclination, as all previous studies are quite limited. This engineering problem is very complex, as it involves 14 input variables. These input variables will be determined in this section. Although the determination of the incident energy is the aim of this study, the equations of several output variables must first be established.

2.1. Identification of input parameters

2.1.1. Location parameters

Several studies have shown the influence of the latitude of a site on the incident solar irradiance in the layout of horizontal single-axis trackers on sloping terrain [19,39].

The extraterrestrial solar irradiance normal to the Earth's surface varies with latitude and longitude due to orbital effects throughout the year. The angle at which the Sun's rays strike the Earth's surface depends on the latitude. Beam solar irradiance at higher latitudes is less than at lower latitudes. On the other hand, the local time at a given location depends on the longitude, which is essential to characterising the daily motion of the Sun.

In addition to latitude, local weather conditions are influenced by altitude and local and regional geography (relief, distance to the sea, etc.). Therefore, the identifier (I_{d1}) will take into account the latitude (λ) and the cloudiness index (k_d), which relates the horizontal diffuse solar irradiance and the horizontal global solar irradiance. The k_d can be used to classify skies, i.e. to define clear, partial and cloudy sky conditions [40].

2.1.2. Sloping terrain parameters

In order to plan the layout of PV modules on a generic sloped terrain, several characteristics of this surface have to be taken into account. The Earth's surface can be flat, sloping, undulating, uneven, etc. These characteristics can be continuous or discontinuous and marked by abrupt, constant or gradual changes. The number of combinations of these characteristics is therefore high. This study will focus on sloping terrain with a constant slope.

Several aspects must be taken into account when classifying sloping terrain, including but not limited to:

- (i) The direction in which a slope is oriented (γ_g) (I_{d2}). This aspect directly determines the amount of solar irradiance received by the sloped surface. The orientation of the slope can be: (a) south, (b) north, (c) east, (d) west, as well as (e) somewhere in between them. This type of orientation will be the subject of this study. A southerly orientation receives the most solar irradiance. The slope orientation is divided into shaded and sunny slopes based on the exposure to light from the slope. This parameter will be another input variable to be considered in this study.
- (ii) The tilt angle of the terrain (α_g) (I_{d3}). This parameter heavily influences on the amount of solar irradiance incident on the solar tracker [19]. Therefore, it will also be taken into account.

Other sloping terrain parameters also influence the layout of PV modules: the available sloping terrain surface and the sloping terrain shape. In this study, however, the slope is considered to be relatively homogeneous in area and continuously distributed.

2.1.3. Horizontal single-axis tracker parameters

The components of a horizontal single-axis tracker are: the structural system (columns, shaft and beams), the transmission system (spherical bearings), the drive device (DC motor and drivers) and the control system. Fig. 3 shows a photograph of a single-axis tracker.

When designing PV power plants with solar trackers, there must never be any shadows [7]. Therefore, the layout of the PV modules will have to comply with this essential condition.

The input variables related to horizontal single-axis trackers are:

- (i) The configuration of PV modules (1 V, 2 V) (I_{d6}). A horizontal single-axis tracker can support several PV modules configurations, such as 1V, 1H, 2 V and 2H [7]. The letter V (H) refers to the PV module configuration where the PV module length (PV module width) is the reference for the module tilt angle. The number 1 (2) represents the number of consecutive vertical PV modules in each row. These PV module configurations on

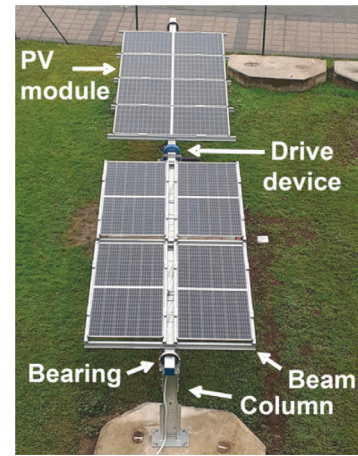


Fig. 3. Photograph of prototype.

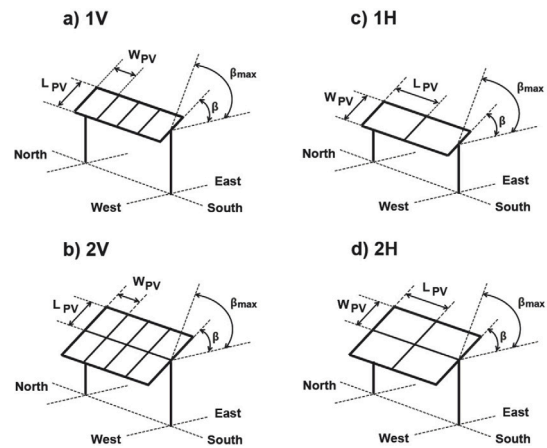


Fig. 4. Configuration of PV modules.

single-axis trackers are shown in Fig. 4. In this figure, L_{PV} is the length of the commercial PV module, and W_{PV} is the width of the commercial PV module. The 1 V and 2 V configurations are the most commonly used in PV power plants [7].

- (ii) The dimensions of commercial PV modules (L_{PV} , W_{PV}) (I_{d7}). The dimensions of a PV module are its length (L_{PV}) and width (W_{PV}). The number of commercial PV modules available on the PV market is very high. For example, Belsky et al. [41] developed a comprehensive study of the technical characteristics of PV modules from the middle of the year 2021 in the power range of 100 to 450 (W). Said study analysed 1300 PV modules.
- (iii) The direction in which the horizontal single-axis tracker is oriented (γ) (I_{d4}). In the northern hemisphere and in a horizontal position, a southerly orientation generates the most energy with horizontal single-axis trackers. Efficiency losses occur if the trackers are not perfectly oriented to the south. When the position is not horizontal, as in this case, an analysis must be done to find the most suitable orientation in order to maximise the solar irradiance received.
- (iv) The tilt angle of the horizontal single-axis tracker (α) (I_{d5}). This parameter greatly influences the amount of solar irradiance incident on the solar tracker [19]. This parameter will be another input variable to be considered in this study.
- (v) The limited range of motion angle (β_{max}) (I_{d8}). For various technical reasons, any given horizontal single-axis tracker have a limited range of motion angles. Each manufacturer has their own

particular design. However, the typical values for this parameter are $\beta_{max} = \pm 60^\circ$ [7].

- (vi) The minimum distance between rows of trackers for the maintenance of the solar field (d_{min}) (Id_9). PV power plants, require inspections, cleaning, and maintenance operations in the PV field, which is why a certain minimum distance between rows of single-axis trackers is established in the design phase of any power plant.
- (vii) The transversal solar angle for avoiding mutual shading in Standard (θ_{st}) (Id_{10}). Certain spacing between trackers is necessary to avoid shading between rows of PV modules. Different countries have different laws requiring minimal spacing between rows of PV modules to minimise shading between rows [42,43]. For example, regulations in Spain state that the distance between rows of PV modules must guarantee a minimum of 4 (h) of sunshine around noon during the winter solstice with no shading between PV modules [42]. This criterion is used by several authors [44,45]. For ease of calculation, this distance is associated with a certain transverse angle θ_{st} .
- (viii) The inter-row spacing (e_r) (Id_{11}). Input variables (β_{max}), (d_{min}) and (θ_{st}) influence the choice of inter-row spacing. This parameter plays a very important role in the design phase of any power plant since poorly designing this parameter can lead to lower power production and can even damage the PV modules due to development of hot spots. Increasing the distance between the rows of trackers eliminates the effect of shading, but increases the initial investment costs (the cost of land, civil engineering work, wiring, etc.). Parameters (β_{max}), (d_{min}) and (θ_{st}) must be met simultaneously for optimal inter-row spacing. The process of choosing the inter-row spacing is complicated because there are several possible cases [14].
- (ix) The periods of operation of a horizontal single-axis tracker (Id_{12}), (Id_{13}), and (Id_{14}). A solar tracker can operate in three different modes [14]: backtracking mode, static mode, and normal tracking mode.

In summary, the main conditions to be fulfilled are:

- The movement must ensure that there are no shadows [7]. When the solar elevation is low, i.e. at sunrise and sunset, the solar tracker uses the so-called backtracking movement to avoid shadows [25]. As the usual installation of horizontal single-axis trackers is on a horizontal surface, equations have been developed that define the backtracking mode for this type of surface [14]. However, these equations cannot be used when the terrain is oriented in any direction and with any inclination, as they do not completely avoid shading between rows of horizontal single-axis trackers [29]. The determination of the equation defining the backtracking tilt angle (β_B), the start (T_{b2}) and end (T_{b1}) times of this period of operation, will be variables under study.
 - Horizontal single-axis trackers have a limited rotation range, $\pm\beta_{max}$. When the tracker reaches this value, the tracker stops, remaining in the static mode of operation until the other modes of operation begin. The duration of this period of time will depend on the location and the day of the year.
 - Finally, as regarding the layout, there is a distance between rows to allow maintenance (d_{min}), and a distance to guarantee the standard IDAE [42], expressed as a function of (θ_{st}).

In normal tracking mode, the motion of the horizontal single-axis tracker is defined by β . This angle is determined to maximise the cosine of the solar incidence angle [23]. To do this, the control system matches the tracker rotation to the projection of the Sun's position on the tracker plane of rotation. The equation defining β , as well as the start ($T_{\beta 1}$) and end ($T_{\beta 2}$) times of this operating period must be determined for the control system. Depending on the location and the day of the year, you may or may not be able to use all three modes of operation [14]. Each mode of operation is governed by a specific equation. This is one of the objectives of this paper. Fig. 5 shows an example of the three periods of operation.

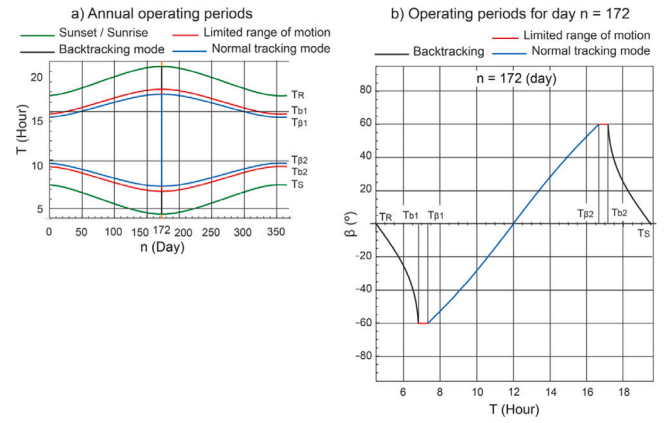


Fig. 5. Periods of operation of a horizontal single-axis tracker.

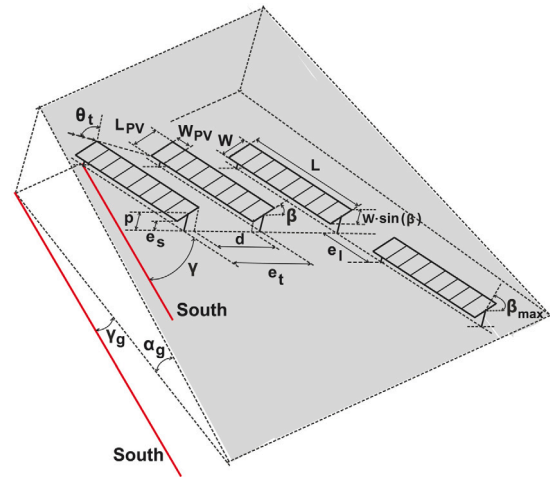


Fig. 6. Photovoltaic power plant design parameters.

2.1.4. Summary of input parameters

Table 1 lists the variables that need to be known in order to design a PV power plant. Fig. 6 shows these parameters.

Some of these input variables are related to each other, which further complicates the matter. All these input parameters are needed to maximise the annual incident energy on the PV field, which is the ultimate goal of any PV power plant design. Commercial software is available to model a PV power plant with horizontal single-axis trackers oriented in any direction and any slope. For example: PVsyst [36], SolarFarmer [37], RETScreen [38], etc. The layout of the solar trackers has to be entered into these programs as the main data. Such process is highly complicated given the large number of input variables. The work presented here facilitates this task by optimising the layout of the solar trackers on the available land.

3. Methodology

The proposed methodology focuses on determining three factors: (i) the equations defining the correct solar tracker motion operation, (ii) the solar tracker operating periods, and (iii) the optimal choice of solar tracker layout on a sloping terrain oriented in any direction. Fig. 7 shows a flow chart summarising the proposed methodology.

This methodology has been used to establish these equations based on the following steps: (i) coordinating system deduction, (ii) deducing the relationship between the sloping terrain angles (α_g and γ_g) and the solar tracker angles (α and γ), (iii) transforming the reference system S' into the system S'' , (iv) the inter-row spacing design, (v) determining

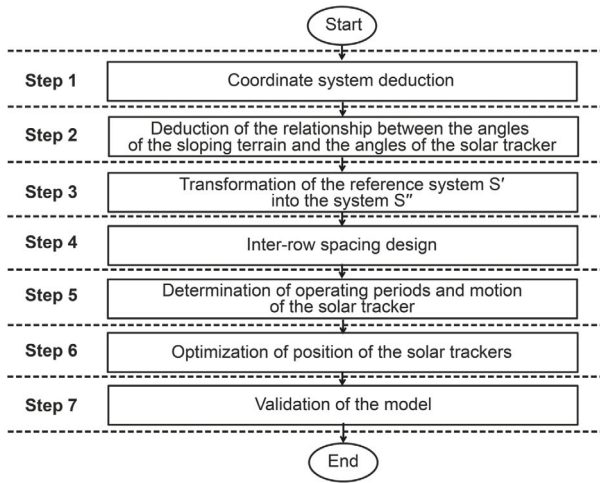


Fig. 7. A flowchart outlining the proposed methodology.

the operating periods and motion of the solar tracker, (vi) optimising the position of the solar trackers, and (vii) validating of the model.

3.1. Coordinating system deduction

One of the most important aspects of this methodology is the appropriate choice of the reference system. Two reference systems can be used to determine the equations governing the motion of a horizontal-axis tracker deployed on a horizontal surface:

- (i) The global reference system (S). This reference system uses the centre of the Earth as the origin and is characterised by [23]: (a) the Oxy plane coinciding with the equatorial plane; (b) the Oz axis being the axis of rotation; (c) the Ozy plane coinciding with the meridian plane of the site. The Ox axis is the vector product of the $Oy \times Oz$ axes, and is therefore perpendicular to the Ozy plane in a westerly direction. The position of the Sun in this system is given by two coordinates: the solar declination (δ) and the hour angle (ω). The corresponding can be found in [23].
- (ii) The local reference system (S') (see Fig. 10). This reference system uses the solar tracker located on the Earth's surface as the origin. This local reference system is characterised by [23]: (a) the Ox' axis points west; (b) the Oy' axis points south; (c) the Oz' axis points towards the zenith. The position of the Sun in this system is given by two coordinates: the solar altitude (α_s) and solar azimuth (γ_s). The corresponding equations can be found in [23]. This reference system (S') is used in horizontal single-axis tracker surveys deployed on a horizontal surface [14].

As this paper analyses a terrain slope oriented in any direction, the reference system (S') is not the most appropriate. A new reference system linked to the solar tracker axis (S'') was already used in a paper [19] devoted to the study of horizontal single-axis trackers deployed on sloping terrain and oriented north–south. The reference system (S'') was obtained by rotating the reference system (S'). This technique will be used in the work presented here. Fig. 8 shows the reference systems (S'') and (S').

The solar tracker array in this figure is represented by the solar trackers T_1 and T_2 . The concept of the line of greatest slope (LGS) of a plane surface will be used in this study. LGS is the line of the plane that develops the greatest angle of the plane with respect to the horizontal plane of projection (Ox', Oy') of the reference system (S'), and is therefore perpendicular to the horizontal trace of the plane. As mentioned above (see Table 1), the position of the sloping terrain is defined by the angles: γ_g (Id_2) and α_g (Id_3), and the position of the

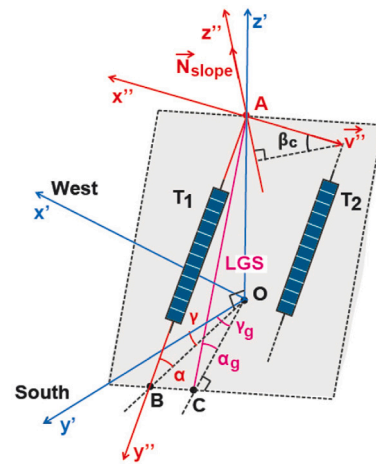


Fig. 8. Reference systems (S') and (S'').

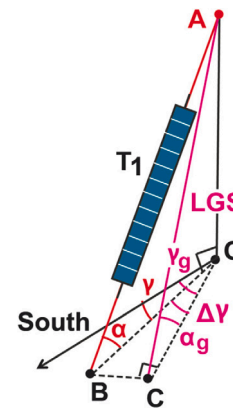


Fig. 9. Detail of angles.

solar tracker by the angles: γ (Id_4) and α (Id_5).

These angles can be defined with respect to the reference system (S'):

- (i) γ_g is the angle between the horizontal projection of the LGS of the tilted terrain and the south axis (Oy'). The following sign convention was used: $\gamma_g < 0$ ($\gamma_g > 0$) if the sloping terrain is turned to the east (west).
- (ii) α_g is the angle between the LGS of the sloping terrain and its projection onto the horizontal plane of projection (Ox', Oy') of the reference system (S'). The sign convention used was as follows: $\alpha_g > 0$ ($\alpha_g < 0$) if the slope goes up (down) from south to north.
- (iii) γ is the angle between the horizontal projection of the tracker axis and the South axis (Oy'). The following sign convention was used: $\gamma < 0$ ($\gamma > 0$) if the tracker is turned to the east (west).
- (iv) α is the angle between the tracker axis and its projection onto the horizontal plane of projection (Ox', Oy') of the reference system (S'). The sign convention used was as follows: $\alpha > 0$ ($\alpha < 0$) if the tracker goes up (down) from south to north.

The sign criteria for γ_g and γ were chosen to be consistent with the criterion that the solar azimuth $\gamma_s < 0$ before noon while after noon, $\gamma_s > 0$. And, the sign criteria for α_g and α were chosen to be consistent with the criterion that the solar height is $\alpha_s > 0$.

A new reference system (S'') linked to the axis of the tracker must be used to the characteristics of the sloping terrain (see Fig. 8). The reference system (S'') can be defined as follows:

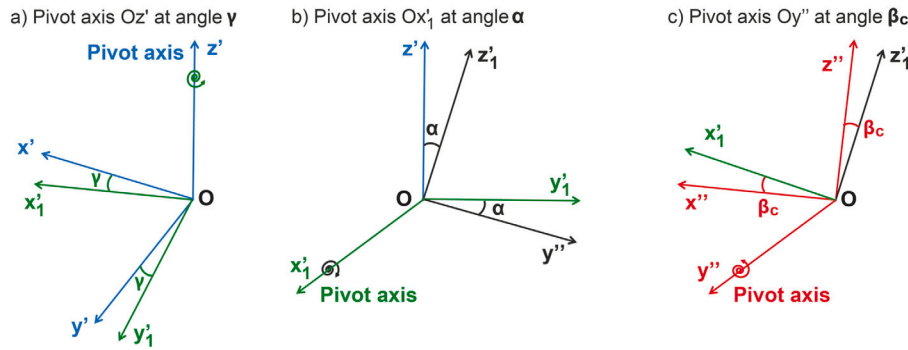


Fig. 10. Transformation of the reference system (S') into the system (S'').

- (i) The Oy'' axis is the straight line defining the tracker axis. The positive direction of the Oy'' axis is towards the south.
- (ii) The Oz'' axis is the normal to the sloped terrain (\vec{N}_{slope}). The positive direction of the Oz'' axis is towards the zenith.
- (iii) The Ox'' axis was determined by the vector product of the axes Oz'' and Oy'' , $Oz'' \times Oy''$. The positive direction of the Ox'' axis is towards the west.

3.2. Relationship between the sloping terrain angles and the solar tracker angles

The relationship between the sloping terrain angles (α_g and γ_g) and the solar tracker angles (α and γ) can be deduced from Fig. 9. The parameters $\Delta\gamma$ and α can be defined as:

$$\Delta\gamma = \gamma_g - \gamma \quad (1)$$

$$\alpha = \arctan(\tan \alpha_g \cos(\gamma_g - \gamma)) \quad (2)$$

Eq. (2) is fundamental to optimising the layout of the solar trackers on the sloping terrain. In other words, the optimal design objective for a given sloping terrain, defined by (α_g , γ_g), is the optimal choice of (α , γ) for the solar trackers. According to relationship (2), only one degree of freedom is available; therefore, the objective will be to calculate the optimal angle γ that completely defines the solar tracker system.

3.3. Transforming the reference system S' into the system S''

The matrices that allow the reference system (S'') to be obtained from the reference system (S') must be determined (see Fig. 10).

The reference system (S'') can be obtained from the reference system (S') by means of three rotations, according to the sequence: blue (S') (Pivot axis Oz' at angle γ , see Fig. 10a) \rightarrow green (Pivot axis Ox'_1 at angle α , see Fig. 10b) \rightarrow black (Pivot axis Oy'' at angle β_c , Fig. 10c) \rightarrow red (S''). Each of these rotations will be discussed below.

1st rotation: rotation around the Oz' axis by an angle γ .

With this rotation, the reference system (S') rotates around the Oz' axis by an angle γ . The rotation matrix is as follows:

$$M_{z'} = \begin{pmatrix} \cos \gamma & -\sin \gamma & 0 \\ \sin \gamma & \cos \gamma & 0 \\ 0 & 0 & 1 \end{pmatrix} \quad (3)$$

The matrix $M_{z'}$ transforms the reference system (S') (Ox' , Oy' , Oz') to the green reference system (Ox'_1 , Oy'_1 , Oz'_1). As the chosen sign convention is $\gamma < 0$, the matrix corresponds to a counterclockwise rotation.

2nd rotation: rotation around the Ox'_1 axis by an angle α

With this rotation, the green reference system rotates around the Ox'_1 axis by an angle α . The rotation matrix is as follows:

$$M_{x'_1} = \begin{pmatrix} 1 & 0 & 0 \\ 0 & \cos \alpha & -\sin \alpha \\ 0 & \sin \alpha & \cos \alpha \end{pmatrix} \quad (4)$$

The matrix $M_{x'_1}$ transforms the green reference system (Ox'_1 , Oy'_1 , Oz'_1) to the black reference system (Ox''_1 , Oy''_1 , Oz''_1). As the chosen sign convention is $\alpha > 0$, the matrix corresponds to a clockwise rotation. The rotation matrix M_{12} of the first two rotations can be expressed as:

$$M_{12} = M_{x'_1} \cdot M_{z'} \quad (5)$$

The rotation matrix (5) takes into account the parameters γ and α .

3rd rotation: rotation around the Oy'' by an angle β_c

With this rotation, the black reference system rotates around the Oy'' axis by an angle β_c . β_c is the tilt angle between rows of solar trackers referred to the black system (see Fig. 8). The rotation matrix is as follows:

$$M_{y''} = \begin{pmatrix} \cos \beta_c & 0 & -\sin \beta_c \\ 0 & 1 & 0 \\ \sin \beta_c & 0 & \cos \beta_c \end{pmatrix} \quad (6)$$

The matrix $M_{y''}$ transforms the black reference system (Ox''_1 , Oy''_1 , Oz''_1) to the reference system (S'') (Ax'' , Ay'' , Az''). As the chosen sign convention is $\beta_c > 0$, the matrix corresponds to a counterclockwise rotation.

The angle β_c can be calculated by the vector \vec{v}'' (see Fig. 8). The vector \vec{v}'' is the vector product of the normal to the sloping terrain (\vec{N}_{slope}) and the axis Ay'' :

$$\vec{v}'' = \vec{N}_{slope} \times Ay'' \quad (7)$$

These two vectors referring to the reference system (S') can be expressed:

$$\vec{N}_{slope} = (\sin \alpha_g \sin \gamma_g, \sin \alpha_g \cos \gamma_g, \cos \alpha_g) \quad (8)$$

$$Ay'' = (\cos \alpha \sin \gamma, \cos \alpha \cos \gamma, -\sin \alpha) \quad (9)$$

And by means of the matrix M_{12} they can be referred to the black reference system (Ox''_1 , Oy''_1 , Oz''_1):

$$\vec{v}'' = M_{12} \cdot (\vec{N}_{slope} \times Ay'') \quad (10)$$

Therefore, the tilt angle between rows of trackers β_c , is:

$$\beta_c = \arcsin(\vec{v}''_{z''}) \quad (11)$$

Thus, $|\vec{v}''| = 1$. The vector \vec{v}'' is directed along the axis $-Ax''$.

The total rotation matrix for moving from the reference system (S') (Ox' , Oy' , Oz') to the reference system (S'') (Ax'' , Ay'' , Az'') is therefore:

$$M = M_{y''} \cdot M_{12} \quad (12)$$

The rotation matrix (12) takes into account the parameters γ , α and β_c .

Finally, the values of the Sun must be expressed in the reference system (S''). The solar vector with respect to the local system (S') is given by the classical expression [23]:

$$\vec{n}'_S = (\sin \gamma_s \cos \alpha_s, \cos \gamma_s \cos \alpha_s, \sin \alpha_s) \quad (13)$$

$$= (\sin \omega \cos \delta, \cos \omega \cos \delta \sin \lambda - \sin \delta \cos \lambda, \cos \omega \cos \delta \cos \lambda + \sin \delta \sin \lambda) \quad (14)$$

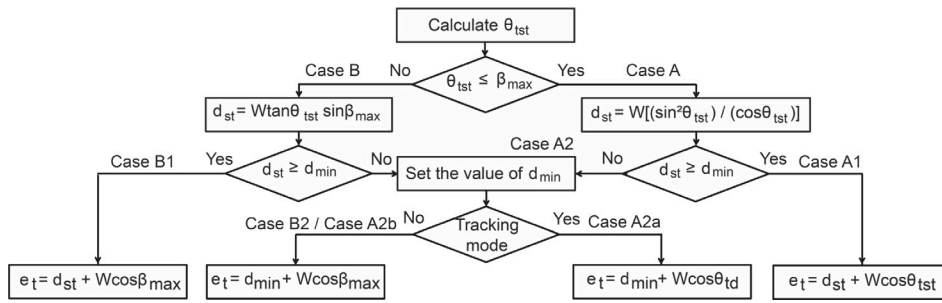


Fig. 11. Flowchart for different cases of inter-row design on a horizontal surface.

where α_S is the height angle of the Sun ($^\circ$), γ_S is the azimuth of the Sun ($^\circ$), δ is the solar declination ($^\circ$), λ is the latitude ($^\circ$), and ω is the hour angle ($^\circ$). And the solar vector in the new reference system (S'') is:

$$\vec{n}_S'' = M \cdot \vec{n}_S' \quad (15)$$

The normal terrain (pointing away from the Earth) to the surface of the PV module \vec{n}_p'' in the reference system (S'') is given by:

$$\vec{n}_p'' = (\sin \beta, 0, \cos \beta) \quad (16)$$

where the plane of rotation of the solar tracker is the plane (Ox'' , Oz'') of the reference system (S'') and β is the rotation angle of the solar tracker ($^\circ$). β is the angle between \vec{n}_p'' and Az'' .

The incident angle θ , which is the angle between \vec{n}_S'' and the normal terrain to the surface of the PV module \vec{n}_p'' is given by:

$$\cos \theta = \frac{\vec{n}_S'' \cdot \vec{n}_p''}{|\vec{n}_S''| \cdot |\vec{n}_p''|} \quad (17)$$

Vectors \vec{n}_S'' and \vec{n}_p'' are unit vectors. Therefore:

$$\cos \theta = \vec{n}_S'' \cdot \vec{n}_p'' = (\vec{n}_S'')_x \sin \beta + (\vec{n}_S'')_z \cos \beta \quad (18)$$

In normal tracking mode, priority is given to maximising the incident beam solar irradiance over the PV field. For this purpose, angle β must be such that the projection of \vec{n}_S'' on the plane perpendicular to the PV field is parallel to the \vec{n}_p'' [23]. This shall be called the *optimal pointing condition*, and is given by the equation:

$$\beta = \theta_t'' = \arctan \left[\frac{(\vec{n}_S'')_x}{(\vec{n}_S'')_z} \right] \quad (19)$$

where θ_t'' ($^\circ$) is the transversal angle in the reference system (S''). The sign convention used is: $\theta_t'' < 0$ before noon and $\theta_t'' > 0$ after noon.

Simply by operating properly, β can be eliminated and a compact equation can be obtained for the cosine incidence angle under optimal pointing (i.e. normal tracking mode) from the Eqs. (18) and (19):

$$\left. \begin{aligned} \cos \theta &= (\vec{n}_S'')_x \sin \beta + (\vec{n}_S'')_z \cos \beta \\ \tan \beta &= \frac{(\vec{n}_S'')_x}{(\vec{n}_S'')_z} \end{aligned} \right\} \rightarrow \cos \theta = \sqrt{(\vec{n}_S'')_x^2 + (\vec{n}_S'')_z^2} \quad (20)$$

The main advantage of operating in the reference system (S'') is that it places the solar trackers deployed on a horizontal surface. To do so, the solar tracker must be positioned with its axis of rotation parallel to the sloped terrain, i.e. taking into account β_c . Therefore, this is the reference system used in this study. The convention for the slope of the inclined terrain with respect to the horizontal will be: (i) $\beta_c > 0$ if the slope decreases from east to west (clockwise), and (ii) $\beta_c < 0$ if the slope increases from east to west (counter clockwise). This convention is consistent with the convention set for θ_t , and β .

Throughout the rest of the paper, all of the calculations are referred to the new reference system S'' .

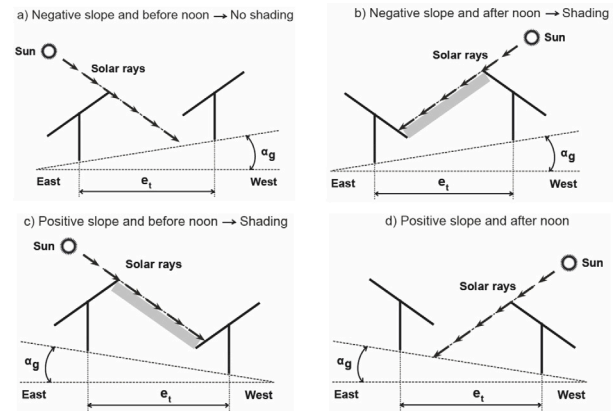


Fig. 12. Cases according to the sign α_g and the position of the Sun.

3.4. Inter-row spacing design

Achieving optimal inter-row spacing is a fundamental and complex task when designing PV power plants. Some authors have addressed this issue with different terrain topographies. Considering certain simplifications, Anderson [29] studied inter-row spacing on a sloping terrain in the east–west direction with the solar trackers deployed in the north–south direction. The conclusions of his work cannot be applied to the study presented here.

Several papers have approached the issue of horizontal terrain; however, the most complete research work was published by [14]. Said paper considers the three aforementioned conditions (β_{max} , d_{min} and θ_{tst}) that must be fulfilled simultaneously to optimise inter-row spacing and classifies inter-row spacing design into five possible cases. The derived equations obviously cannot be applied to the work presented here, but the procedure used can be considered a starting point. Fig. 11 shows a flowchart describing the possible cases for solar trackers deployed on a horizontal surface [14]. If the terrain is inclined in a north–south direction, the solution is the same as for horizontal terrain [19].

The difference between horizontal terrain and sloping terrain oriented in any direction will be analysed below. For the sake of simplicity, yet without losing any generality, we shall present one particular case (see Fig. 2c): the case of an increasing slope from east to west. The conclusions obtained from the study carried out based on this example are easily generalisable to the general case. Fig. 12 shows several explanatory examples.

Here is one:

- (i) There are two possible considerations depending on the orientation of the sloping terrain, the slope of the terrain, and the position of the Sun (before or after noon). With the first, known as

Table 2
Study data for the choice of e_t .

Location	Almeria (Spain); Latitude: 36°50'07" N; Longitude: 02°24'08" W; Altitude: 22 (m)
Land	Slope orientation: E-W; Crescent from East to West; $\beta_c = -10$ (°)
PV module	LR5-72HBD 535; 535 (Wp); dimensions: 1133 × 2256 (mm)
β_{\max}	60 (°)
d_{\min}	4 (m)
e_t	0.3 (m)
Example 1	1V; n_p : 60; W: 2.256 (m); L: 69.455 (m)
Example 2	2V; n_p : 120; W: 4.537 (m); L: 69.455 (m)

“favourable”, less e_t spacing is needed to avoid shading between rows. On the other hand, with the second, which is thought to be “unfavourable”, more spacing e_t is needed. In our example the unfavourable consideration is clearly after noon.

- (ii) Equations have been defined for horizontal surfaces to determine the time of sunrise ($T_R(n)$) and sunset ($T_S(n)$) [23] (n is the day of the year). These equations do not apply to sloping terrain as there must be verification of whether the Sun goes down behind the sloping terrain. Therefore, in the new reference system (S''), the equations for the calculation of sunrise and sunset are not the same as when the surface is horizontal. Thus, the new sunrise and sunset must be calculated according to the orientation and inclination of the terrain. The first step is to verify whether the Sun is hidden in the interval [$T_R(n)$, $T_S(n)$] behind the tilted terrain, i.e. whether the cosine of the angle between the normal to the sloped terrain (\vec{N}_{slope}) and the normal to the Sun \vec{n}_S'' is positive. This will provide a new working interval: [$T_R^*(n)$, $T_S^*(n)$].

Taking into account all of the above considerations, the choice of e_t can be made in two ways:

- (i) **Mode I.** Choose the “unfavourable” consideration (before or after noon, depending on the slope steepness) and then impose step e_t following the steps proposed in [14] for a horizontal surface (see Fig. 11). The process is by no means trivial as all 5 cases (see Fig. 11) [14] may be true for the unfavourable consideration (before or after noon). Then, pitch e_t is set for the favourable consideration (before or after noon) and e_t will be generally over dimensioned.
- (ii) **Mode II.** Choose e_t considering that the surface is horizontal [14]. In this study, it would also be necessary to consider the 5 possible cases [14] (see Fig. 11). This e_t is always smaller than in Mode I, and the problem is greatly simplified.

The advantages and disadvantages of using Mode I or II will be discussed below.

With Mode I, the most ‘unfavourable’ option is chosen for the determination of e_t . This most ‘unfavourable’ option can be fulfilled before or after noon, depending on the slope steepness (see Fig. 12). In contrast, with Mode II, the surface is considered to be horizontal. Mode II is obviously more straightforward as there are no prior calculations to be made in order to apply it. The procedure for determining e_t on a horizontal surface has been detailed in [14].

Regardless of whether Mode I or Mode II is used, five different cases can be given depending on β_{\max} , d_{\min} , and θ_{1st} . Fig. 11 shows these cases [14].

Two examples were carried out to compare the results of the application of the proposed procedure in Mode I and Mode II when determining e_t . Table 2 shows the data from this study.

In Example 1 for $n = 355$, e_t is 5.28 (m) in the most ‘unfavourable’ Mode I option. And it is 5.128 (m) in Mode II. The operating periods shown in Table 3 were obtained with these results.

In Mode I with the calculated e_t , $T_{b2} - T_{b1} = 5.98$ (h), meaning more than 4 (h) are being imposed on the 355th day. In Mode II with the calculated e_t , $T_{b2} - T_{b1} = 5.87$ (h), so more than 4 (h) are also being imposed on the 355th day. Therefore, all three conditions (β_{\max} , d_{\min} and θ_{1st}) are satisfied with either of the two modes.

Table 3
Operating periods for Example 1 (1V), $n = 355$.

Operating period	Mode I		Mode II	
	Start	End	Start	End
	Time (h)	Time (h)	Time (h)	Time (h)
Sunrise backtracking mode	$T_R = 7.26$	$T_{b1} = 8.33$	$T_R = 7.26$	$T_{b1} = 8.40$
Static mode	$T_{b1} = 8.33$	$T_{\beta1} = 9.40$	$T_{b1} = 8.40$	$T_{\beta1} = 9.40$
Normal tracking mode	$T_{\beta1} = 9.40$	$T_{b2} = 14.32$	$T_{\beta1} = 9.40$	$T_{b2} = 14.27$
Sunset backtracking mode	$T_{b2} = 14.32$	$T_S^* = 15.94$	$T_{b2} = 14.27$	$T_S^* = 15.94$

Table 4
Operating periods for Example 2 (2V), $n = 355$.

Operating period	Mode I		Mode II	
	Start	End	Start	End
	Time (h)	Time (h)	Time (h)	Time (h)
Sunrise backtracking mode	$T_R = 7.26$	$T_{b1} = 8.80$	$T_R = 7.26$	$T_{b1} = 9.39$
Static mode	$T_{b1} = 8.80$	$T_{\beta1} = 9.40$	$T_{b1} = 9.39$	$T_{\beta1} = 9.40$
Normal tracking mode	$T_{\beta1} = 9.40$	$T_{b2} = 14.00$	$T_{\beta1} = 9.40$	$T_{b2} = 13.56$
Sunset backtracking mode	$T_{b2} = 14.00$	$T_S^* = 15.94$	$T_{b2} = 13.56$	$T_S^* = 15.94$

Table 5
Results of the study for the choice of e_t .

Parameter	Example 1 (1V)		Example 2 (2V)	
	Mode I	Mode II	Mode I	Mode II
H_a (MWh/m ²)	2.3183	2.3124	2.2734	2.2039
a_{PV} (m ²)	153.36	153.36	306.72	306.72
E_a (MWh)	355.54	354.64	697.3	675.99
a_t (m ²)	368.92	357.70	605.89	485.35
EAR (MWh/m ²)	0.963	0.991	1.150	1.392

In Example 2 where $n = 355$, e_t is 8.68 (m) in the most ‘unfavourable’ Mode I option. And it is 6.95 (m) in Mode II. The operating periods shown in Table 4 were obtained with these results.

In Mode I, with the calculated e_t , $T_{b2} - T_{b1} = 5.20$ (h), meaning more than 4 (h) are being imposed on the 355th day. In Mode II with the calculated e_t , $T_{b2} - T_{b1} = 4.16$ (h), so more than 4 (h) are being imposed on the 355th day. Therefore, all three conditions (β_{\max} , d_{\min} and θ_{1st}) are satisfied in the two modes.

The assessment indicators of this study are: (i) the annual solar irradiation incident on the PV field (H_a) (using Eq. (34)), (ii) the area required for the deployment of the solar trackers (a_t) ($a_t = e_t \cdot (L + e_t)$), (iii) the annual energy (E_a) ($E_a = a_t \cdot H_a$), and (iv) the EAR (the ratio between the annual energy incident on the PV field (E_a) and the area occupied by the PV field (a_t)) [46]. Table 5 shows the results obtained in these two examples.

The following conclusions can be drawn based on the results shown in Table 5:

- Mode I leads to slightly better results in solar irradiance and therefore in the incident energy on the PV field.
- Mode II requires less surface area for installation. This fact is more noticeable in the 2 V configuration.
- As far as the EAR parameter is concerned, Mode II clearly performs better. This is most noticeable in the 2 V configuration.

Table 6
Periods of operation with a horizontal single-axis tracker in the most general case.

Operating period	Start		End		Motion	Incidence
	Time	Angle	Time	Angle		
Sunrise backtracking mode	$T_R^*(n)$		$T_{b_1}(n)$	θ_{tb1}	β_B	$\cos \theta_B$
Static mode	$T_{b_1}(n)$	θ_{tb1}	$T_{\beta}(n)$	$\theta_{t\beta1}$	$-\beta_{\max}$	$\cos \theta_S$
Normal tracking mode	$T_{\beta}(n)$	$\theta_{t\beta1}$	$T_{\beta_2}(n)$	$\theta_{t\beta2}$	θ_t	$\cos \theta$
Static mode	$T_{\beta_2}(n)$	$\theta_{t\beta2}$	$T_{b_2}(n)$	θ_{tb2}	β_{\max}	$\cos \theta_S$
Sunset backtracking mode	$T_{b_2}(n)$	θ_{tb2}	$T_S^*(n)$		β_B	$\cos \theta_B$

Therefore, the use of Mode II is recommended as the best option, for determining e_t , when the surface is considered to be horizontal. Therefore, the pitch in the reference system (S'') can be determined by the equation:

$$e_t'' = \frac{e_t}{\cos \beta_c} \quad (21)$$

where e_t is the pitch that would be imposed on horizontal terrain.

3.5. Determining operating periods

In general, there are three periods of operation with a horizontal single-axis tracker: backtracking mode, static mode and normal tracking mode. Nonetheless, there are sometimes only two: backtracking mode and normal tracking mode. Table 6 lists the periods of operation for the most general case.

Each period of operation is associated with a certain solar tracker motion. Knowledge of the parameters shown in Table 2 is essential for defining the solar tracking algorithm and calculating the incident energy on the PV field.

3.5.1. Solar tracker movement

The equations governing the movement of the solar tracker in the three periods of operation will be deduced in this section. The equations governing each mode of operation are as follows:

- (i) Determination of β in backtracking mode. β_B and $\cos \theta_B$ in the reference system (S'') can be determined by the equations:

$$\beta_B = \theta_t'' + \theta_c'' = \theta_t'' - \text{sign}(\theta_t'') \arccos\left(\frac{e_t''}{W} \cos \theta_t''\right) \quad (22)$$

$$\cos \theta_B = \vec{n}_S'' \cdot \vec{n}_p'' = (\vec{n}_S'')_x \sin \beta_B + (\vec{n}_S'')_z \cos \beta_B \quad (23)$$

- (ii) Determination of β in static mode. β_S and $\cos \theta_S$ in the reference system (S'') can be determined by the equations:

$$\beta_S = \pm \beta_{\max} \quad (24)$$

$$\cos \theta_S = \vec{n}_S'' \cdot \vec{n}_p'' = (\vec{n}_S'')_x \sin(\text{sign}(\omega)\beta_{\max}) + (\vec{n}_S'')_z \cos(\text{sign}(\omega)\beta_{\max}) \quad (25)$$

- (iii) Determination of β in normal tracking mode. β and $\cos \theta$ in the reference system (S'') can be determined by the equations:

$$\beta = \theta_t'' \quad (26)$$

$$\cos \theta = \sqrt{(\vec{n}_S'')_x^2 + (\vec{n}_S'')_z^2} \quad (27)$$

3.5.2. Solar tracker operating periods

The equations that determine the operating periods are as follows:

- (i) Determination of $T_R^*(n)$ and $T_S^*(n)$. The sunrise ($T_R^*(n)$) and sunset ($T_S^*(n)$) reflect changes when compared to cases of horizontal terrain ($T_R(n)$, $T_S(n)$), due to the slope of the terrain. As already mentioned, these conditions are used to calculate these instants if the cosine of the angle between the normal to the inclined terrain (\vec{N}_{slope}) and the normal to the Sun \vec{n}_S'' is positive.

- (ii) Determination of $T_{\beta_1}(n)$ and $T_{\beta_2}(n)$. In order to calculate the instants where normal tracking mode changes to static mode, you simply must consider the two values of the solar time T_{β} obtained from the equation:

$$\theta_t'' = \pm \beta_{\max} \quad (28)$$

- (iii) Determination of $T_{b_1}(n)$ and $T_{b_2}(n)$. As the backtracking mode can evolve into static mode or normal tracking mode, only two cases can now arise. From the study presented in [14]:

$$e_t'' = \frac{W}{\cos(\theta_t'')} \quad (29)$$

and as pitch e_t is fixed, we call θ_{tb} :

$$\theta_{tb} = \text{sign}(\theta_t'') \arccos\left(\frac{W}{e_t''}\right) \quad (30)$$

The only two cases that can now arise are based on the value of θ_{tb} in Eq. (30):

$$\text{Case I : } |\theta_{tb}| \leq \beta_{\max}$$

$$\text{Case II : } |\theta_{tb}| > \beta_{\max} \quad (31)$$

In Case I the backtracking mode starts in θ_{tb} with the tracker in normal tracking mode, i.e. it starts at (30):

$$\theta_{tb1} = \theta_{tb} \quad (32)$$

In Case II, the backtracking mode starts with the solar tracker in static mode. From the study presented in [14]:

$$e_t'' - W \cos(\beta_{\max}) = W \tan(\theta_t) \sin(\beta_{\max}) \quad (33)$$

and simply solving the previous equation θ_t , a value of θ_{tb2} is obtained.

3.6. Optimising the of position of the solar trackers

The optimisation of the position of the solar trackers on a particular terrain with a general slope involves two phases:

- (1) The optimal choice of (α, γ) for the solar trackers for a given sloping terrain is defined by (α_g, γ_g) . Eq. (2) is used. According to relationship (2), only one degree of freedom is available, therefore the objective will be to calculate the optimal angle γ that completely defines the solar tracker system. The objective in this phase is to maximise the annual incident solar irradiation (H_a) on the PV field:

$$H_a = \sum_{n=1}^{365} H_t(n) \quad (34)$$

where H_a is the annual incident solar irradiation on the PV field (Wh/m^2), and H_t is the daily incident solar irradiation on the PV field (Wh/m^2). To calculate the optimal value of γ , a force brute algorithm is used, calculating the maximum value of H_a , varying (α, γ) between appropriate ranges.

- (2) Once the optimal value of γ is calculated, the equations for designing the inter-row spacing to avoid shading between adjacent PV modules can be derived, and the operating periods of the solar tracker can be determined, a packing algorithm can be used to maximise the total PV modules area (A_{TPV}) using the following parameters: the number of PV modules (N_{PV}), the width of a PV module (W_{PV}), and the length of a PV module (L_{PV}). The target function is:

$$A_{TPV} = \sum_{i=1}^{N_{PV}} W_{PV} \cdot L_{PV} \quad (35)$$

To calculate of $H_t(n)$ in the first phase, the periods of operation deduced above must be taken into account as well as the equations that govern the movement of the solar trackers, on each day n of the year. The general case with 5 zones comprising the operating period is:

$$H_t(n) = \int_{T_{\beta_1(n)}}^{T_{\beta_2(n)}} I_t(n, \beta_B, T) dT + \int_{T_{\beta_1(n)}}^{T_{\beta_2(n)}} I_t(n, -\beta_{\max}, T) dT + \int_{T_{\beta_1(n)}}^{T_{\beta_2(n)}} I_t(n, \theta_t, T) dT + \int_{T_{\beta_2(n)}}^{T_{\beta_3(n)}} I_t(n, \beta_{\max}, T) dT + \int_{T_{\beta_2(n)}}^{T_{\beta_3(n)}} I_t(n, \beta_B, T) dT \quad (36)$$

where I_t is the total incident solar irradiance on the PV field (W/m^2). This solar irradiance can be calculated using the equation proposed by [23]:

$$I_t(n, \beta, T) = I_{bh}(n, T) \cdot \frac{\cos \theta}{\cos \theta_z} + I_{dh}(n, T) \cdot \left(\frac{1 + \cos \beta}{2} \right) + (I_{bh}(n, T) + I_{dh}(n, T)) \cdot \rho_g \cdot \left(\frac{1 - \cos \beta}{2} \right) \quad (37)$$

where $I_{bh}(n, T)$ is the beam solar irradiance on horizontal terrain (W/m^2), $I_{dh}(n, T)$ (W/m^2) is the diffuse solar irradiance on horizontal terrain (W/m^2), n is the day of the year (*day*), θ ($^\circ$) is the incident angle in the reference system (S'') for each operating period ($^\circ$), β is the tilt angle in the reference system (S'') for each operating period ($^\circ$), θ_z is the zenith angle of the Sun in the reference system (S'') ($^\circ$), ρ_g is the ground reflectance (*dimensionless*), and T (h) is the solar time. The reasons for the choice of models used in Eq. (37) are as follows:

- (i) Eq. (37) uses the isotropic model devised by Liu and Jordan [47] to determine the diffuse solar irradiance incident on the PV field. Although there are several models for this calculation, the Liu and Jordan model is used, along with many recent works [48–50], because of the good results [51].
- (ii) It is not possible to accurately calculate the ground reflected irradiance over the PV field [23], due to the large number and nature of the factors influencing it [23]. Eq. (37) uses the isotropic model devised by Liu and Jordan [47] to determine the solar irradiance reflected from the ground on an inclined surface. This model has also been frequently used in similar studies [48–50].

Furthermore, Eq. (37) is based on the knowledge of $I_{bh}(n, T)$ and $I_{dh}(n, T)$. The method presented in [52] is used to determine these solar irradiances, following these steps:

- (i) Step 1: Determination of the beam solar irradiance on a horizontal surface ($I_{bh}(n, T)$), using the Hottel clear-sky model [53].
- (ii) Step 2: Determination of the diffuse solar irradiance on a horizontal surface ($I_{dh}(n, T)$), using the Liu-Jordan clear-sky model [54].
- (iii) Step 3: Recalibration of the clear day models from steps 1 and 2 to the meteorological conditions at the site. The practical validity of the equation (37) is highly dependent on the real values of $I_{bh}(n, T)$ and $I_{dh}(n, T)$, which vary with the meteorological conditions. In other words, a cloudy sky model is needed to reduce the $I_{bh}(n, T)$ and $I_{dh}(n, T)$ obtained with clear day models to the meteorological conditions at the location. The procedure proposed by [52] was used for this purpose. This procedure uses monthly-averaged beam and diffuse solar irradiation for the site under study, averaged over a 10-year period, obtained by satellite from the PVGIS database [55].

As for the second phase, studies [13,14] proposed packing algorithms to optimise the PV field of a PV power plant. In the first study, the packing algorithm was applied to a ground-mounted photovoltaic power plant, and in the second study, it was applied to a single-axis tracking photovoltaic power plant. The packing algorithm proposed in [14] will obviously be used in this research work.

Fig. 13. shows the schematics of a PV power plant with horizontal single-axis trackers in the new reference system S'' . The packing system consists of placing rows of solar trackers in the y'' direction inside the

available land area. The projection of each solar tracker on the $x''y''$ plane was considered to develop of the algorithm. The shape of this projection is a rectangle. All these rectangles R_{ij} have the axis of rotation oriented towards the y'' axis. The equations for this packing algorithm can be found in [14].

The phenomenon of shading between PV modules will never occur as the solar trackers are equipped with the backtracking mode. Therefore, the total area of the PV field, A_{TPV} , is constant.

3.7. Validation of the model

The robustness of the derivative equations is demonstrated in this section by validating them from several perspectives. The validation of the model will be carried out from three perspectives: numerical validation, validation using PVsyst software, and experimental validation.

Several specific codes have been developed with *Mathematica*TM software that implement the equations deduced above. To calculate the incident solar irradiance on the PV field, a code has been developed with *Mathematica*TM software that implements the procedure presented in [52].

3.7.1. Analytical validation

The equations for the horizontal terrain and solar tracker configuration with a north–south orientation are in [14]. As $\beta_c = 0$ ($^\circ$) and if the following is substituted in Eq. (2): (i) $\alpha_g = 0$ ($^\circ$), (ii) $\gamma_g = 0$ ($^\circ$), and (iii) $\gamma = 0$ ($^\circ$), $\alpha = 0$ ($^\circ$). Substituting these values into Eqs. (22) to (27) yields the same equations as those shown in [14].

The equations for the sloping terrain configuration with north–south orientation and solar tracker configuration with north–south orientation and tilted at angle A are in [19]. If the following is substituted in Eq. (2): (i) $\alpha_g = A$ ($^\circ$), (ii) $\gamma_g = 0$ ($^\circ$), and (iii) $\gamma = 0$ ($^\circ$), $\alpha = \alpha_g$ ($^\circ$). Substituting these values into Eqs. (22) to (27) yields the same equations as those shown in [19].

The equations for the sloping terrain configuration with an east–west orientation and solar tracker configuration with a north–south orientation are in [29]. If the following is substituted in Eq. (2): (i) $\alpha_g = \beta_c$ ($^\circ$), (ii) $\gamma_g = -90$ ($^\circ$), and (iii) $\gamma = 0$ ($^\circ$), $\alpha = 0$ ($^\circ$). Substituting these values into Eqs. (22) to (27) yields the same equations as those shown in [29].

Therefore, the equations presented here were validated in the three most characteristic cases.

3.7.2. Validation using PVsyst and mathematica software

PVsyst software [36] is simulation software which is widely used to estimate the performance of PV power plants. This software is recommended by the International Renewable Energy Agency [56]. Although PVsyst software does not optimise PV power plants, it can be used to determine the performance of a power plant once the design parameters of the power plant are known. In this paper, PVsyst software was used to validate the derived equations. PVsyst software is frequently used in studies related to PV systems [57,58].

The location chosen to compare the results obtained using PVsyst software and the *Mathematica*TM software code was the city of Gijón (Spain), headquarters of the Department of Electrical Engineering of the University of Oviedo. This location is characterised by: a latitude of $43^\circ 31' 22''$, a longitude of $05^\circ 43' 07'' W$, and an elevation above sea level of 28 (m).

The concept of energy difference (*SED*) is frequently mentioned in the literature [59,60]. It is used to compare different PV mounting systems, solar tracking systems, etc. In this study, we will compare the results obtained with PVsyst software and with *Mathematica*TM software code implemented in terms of energy difference. The energy difference can be calculated as the difference between the incident energy in the PV field calculated using PVsyst software and the

Table 7
Results obtained with *Mathematica*[™] and with PVsyst software.

Scenario	Alg. inputs		Alg. outputs		<i>Mathematica</i> [™] (MWh/m ²)	PVsyst (MWh/m ²)	<i>SED</i> (%)
	γ_s (°)	α_s (°)	γ (°)	α (°)			
1	0	0	0	0	1.4772	1.4730	-0.30
2	0	21.76	0	21.76	1.5976	1.5779	-1.23
3	0	43.52	0	43.52	1.6297	1.5650	-3.97
4	-10	10	-10	9.93	1.4988	1.5280	1.95
5	-20	5	-20	4.82	1.4667	1.4850	2.61

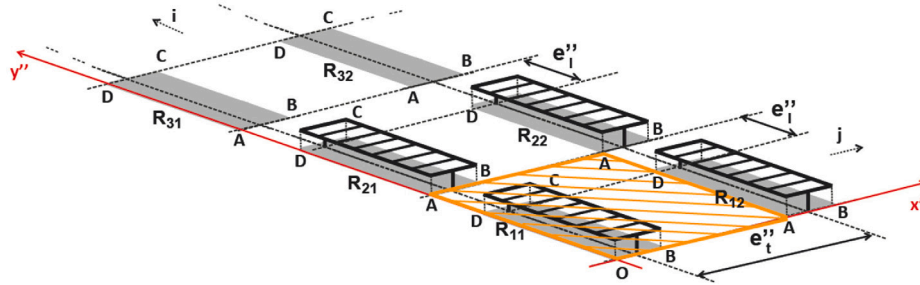


Fig. 13. Packing algorithm in the new reference system S''.

Mathematica[™] software code developed.

$$SED = \frac{H_{aPVs} - H_{aM}}{H_{aM}} \cdot 100 \quad (38)$$

where *SED* is the energy difference due to the software used (%), H_{aPVs} is the annual incident solar irradiation on the PV field calculated with PVsyst software (MWh/m²), and H_{aM} is the annual incident solar irradiation on the PV field calculated with the *Mathematica*[™] software code (MWh/m²).

Table 7 shows some results obtained with the *Mathematica*[™] software code and with PVsyst software. It is remarkable that γ and α are obtained with the proposed optimisation algorithm. The following conclusions can be drawn from Table 7:

- (i) The *Mathematica*[™] software code uses the procedure proposed in [52] based on monthly-averaged beam and diffuse solar irradiation for the site under study, averaged over a 10-year period, obtained by satellite from the PVGIS database [55]. In contrast, the PVsyst software uses the solar irradiation data proposed by Meteonorm 8.0.
- (ii) The results obtained by both procedures are very similar. The difference between the two procedures is largely due to point (i).
- (iii) According to the results obtained, the *Mathematica*[™] software code developed can be considered as validated.

3.7.3. Experimental validation

A prototype of a horizontal single-axis tracker, as illustrated in Fig. 14, was originally manufactured and located at the Department of Electrical Engineering of the University of Oviedo. It consists mainly of the following components: eight PV modules, a DC motor and controllers, and an electronic control module. The measuring equipment includes three identical pyranometers, the specifications of which are as follows: Type TR1 (Kipp & Zonen), a thermopile sensor, range: 0–2000 (W/m²), and precision/resolution: 1 (W/m²). As their characteristics indicate that the uncertainty levels are < 2%, the measurements are considered to be acceptable [61]. The three pyranometers face south, with the following tilt angles: (i) pyranometer 1, with a tilt angle of 0 (°), (ii) pyranometer 2, with a tilt angle equal to half the latitude of the site, and (iii) pyranometer 3, with a tilt angle equal to the latitude of the site. The pyranometers move with the solar tracker's east–west rotation. The traceability of the measurements is ensured by regular calibration of the pyranometers. In addition, pyranometer 4 is used to measure the

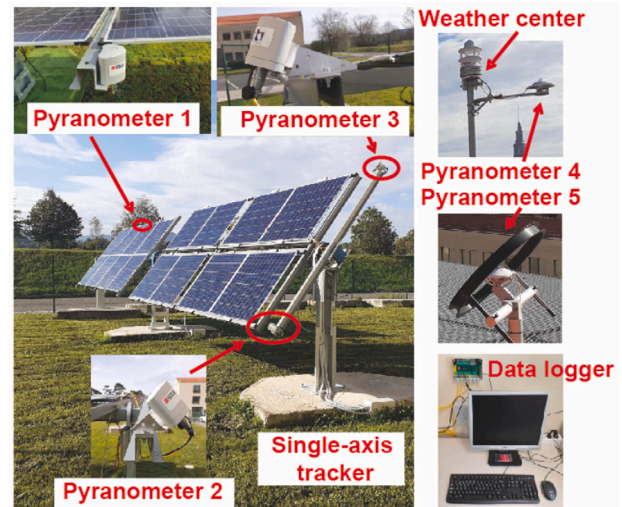


Fig. 14. Configuration of the experimental system.

global solar irradiance on a horizontal surface, and pyranometer 5 is used to measure the diffuse solar irradiance on a horizontal surface.

The test conditions were as follows: (i) the pyranometers take measurements every second with a time step of 1 (min) by integration; (ii) the data collection corresponds to the 12 months of 2022; (iii) only one solar tracker was used, so there was no shading between the solar trackers; and (iv) the tracking mode was not used for the same reason as (iii). Therefore, only two modes of operation were used: static and normal tracking.

In this section, Scenarios 1, 2 and 3 in Table 3 will be compared as a function of the energy gain using the developed *Mathematica*[™] code, the PVsyst software and the experimental results. Fig. 15 shows this comparison. The differences shown in Fig. 15c between the results obtained in the experiment and those obtained with the *Mathematica*[™] code and PVsyst are due to the following factors:

- (i) The test was conducted throughout the year 2022 and the solar irradiance model used data averaged over a 10-year period. For example, in July 2022, higher than average solar irradiance values were obtained, resulting in a monthly energy peak.

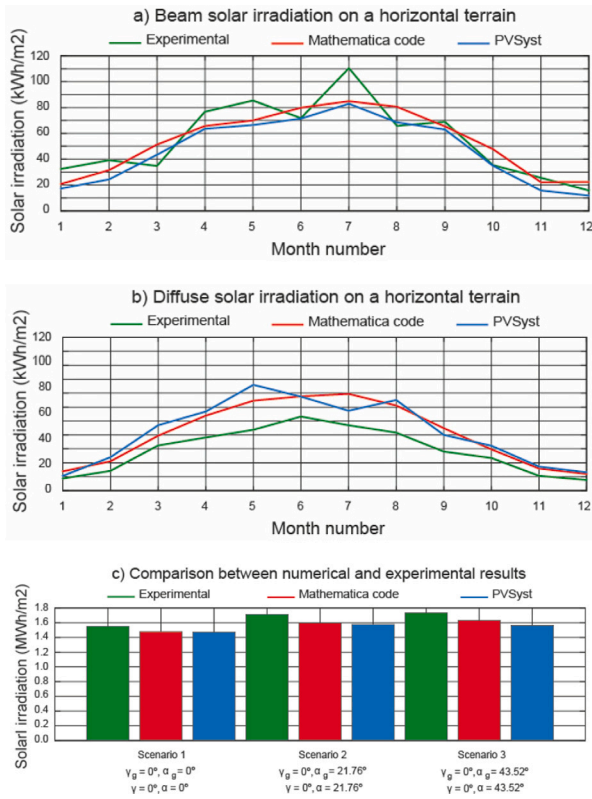


Fig. 15. Comparison: Experimental, *Mathematica*, and PVSystem.

- (ii) The movement of the solar tracker is not continuous; there is certain discretisation. In contrast, the equations used in the *Mathematica*TM code to determine the solar irradiation integrate the solar irradiance, which is a continuous function (The same is true for the PVsystem software.). Therefore, both means lead to differences between them.

Even so, the numerical (*Mathematica*TM and PVsystem) and experimental results are very similar in the three scenarios (see Fig. 15c). Applying the energy difference (*SED*) defined above (see equation (38)) to the experimental results, we obtain: the following *SED*s: for Scenario 1, -4.77% and -5.03%; for Scenario 2, -6.77% and -7.88%; and for Scenario 3, -5.95% and -9.64%. The values are for *Mathematica*TM and PVsystem, respectively on each scenario. These results validate the equations derived and implemented in the *Mathematica*TM code.

3.8. Limitations of the study

Several aspects of *PV* power plant design are the focus of the limitations of this study. These limitations are as follows:

- (i) Limitations related to the maximum angle of movement of the *PV* field. The current study the maximum angle of movement of the *PV* field is $\pm 60^\circ$. If another β_{\max} were used, the results obtained would be different, although the same proposed equations could be used.
- (ii) Limitations related to the availability of meteorological data at the site. The lack of meteorological data for the site studied would make it impossible to calculate the incident irradiance on the *PV* field. However, meteorological data is usually known for most places in the world.

4. Assessment indicators

This section covers the study of the difference between the proposed optimal deployment and a south-facing one. They are analysed from the energetic and economic point of view. A brief analysis of the weather conditions is also included.

4.1. Energy gain

The definition of Energy Gain (*EG*) [46,62] intends to highlight the importance of an energetic study before the deployment of a *PV* system. It represents the difference in incident solar irradiation between an optimally deployed *PV* system, and one southward deployed:

$$EG = H_{a(\gamma_{opt}, \alpha_{opt})} - H_{a(0, \alpha_{opt})} \quad (39)$$

where $H_{a(\gamma_{opt}, \alpha_{opt})}$ is the solar irradiation incident on the optimally deployed field (kWh), and $H_{a(0, \alpha_{opt})}$ is the solar irradiation incident on the southward-oriented (kWh).

4.2. LCOE efficiency

The choice of deployment the economic viability of a system. When the terrain has an orientation other than south, the orientation of the solar tracker affects the profitability of the *PV* system. The economic feasibility study aims to compare the economic performance of the optimally deployed *PV* system to the south-facing one. For *PV* systems, the levelised cost of electricity produced (*LCOE*) is used [63]. It can also be used to compare the costs of different *PV* mounting systems [14,19]. The *LCOE* relates the life cycle cost of the *PV* system to its energetic production. It is computed with the following formula [64]:

$$LCOE = \frac{\sum_{i=0}^N [C_i / (1+r)^i]}{\sum_{i=0}^N [E_i / (1+r)^i]} \quad (40)$$

where *LCOE* is the levelised cost of electricity produced (€/kWh), C_i is the net cost of the project in the i -th year (€), E_i is the total electricity production in the i -th year (kWh), r is the discount rate in the i -th year, N the total lifetime of the project (years), and i is the year ($0 \leq i \leq N$).

4.2.1. Net cost of the project

The net cost of the project comprises: the initial investment cost (the cost of the horizontal single-axis tracker), the operation and maintenance costs, and interest costs (if applicable). In turn, the initial investment includes the costs of the *PV* mounting system, of the *PV* modules, and of the control system and the motor.

The main components of the mounting system are central pillar, the pillars, the shaft and the purlins [14]. The auxiliary ones are the joint shafts, the pillar bearings, the motor brackets, the antenna brackets, the shock absorbers, the end clamps, the clamps, the screws, the nuts, the washers, etc [14]. The weight of the main components is also relevant, and a structural analysis of the *PV* mounting system is necessary to determine it.

The structural design must ensure that the structural capacity of the *PV* mounting system is adequate to support, over its lifetime, its own weight, the weight of the *PV* modules, the weight of accumulated snow, wind loads, or combinations of the above loads. There are mandatory regulations on the action of wind and snow loads on structures in each country. This structural design is carried out using structural analysis software [65]. The main parts of this analysis are:

- (i) Weight of the structure itself.
- (ii) Weight of the *PV* modules. The modules exert a load on the structure (q_{PV}), which depends on their weight (W_{ePV}) and their surface area (A_{PV}). This load can be determined by the equation:

$$q_{PV} = \frac{W_{ePV}}{A_{PV}} \quad (41)$$

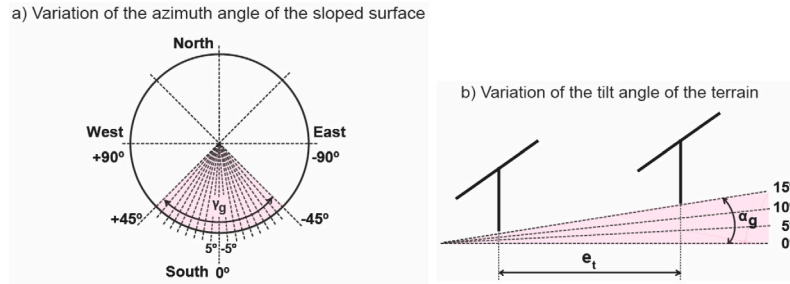


Fig. 16. Range of variation of γ_g and α_g .

- (iii) Weight of accumulated snow, which is determined by equations and parameters defined in the snow load standards of each country (see Table 10), and depends on the latitude, longitude and altitude.
- (iv) Wind loads, also determined by equations and parameters defined in the wind load standards of each country (see Table 10), and depend on the latitude, longitude and altitude, too.
- (v) Combination of the above loads, also detailed in country-specific standards.

The operation and maintenance costs of a horizontal single-axis tracker are set at 0.5% of the initial investment cost according to a report by the National Renewable Energy Laboratory [66].

4.2.2. Total electricity production

The following formula gives the total electricity production in year i :

$$E_i = (\tau \cdot \alpha)_i \cdot H_i \cdot \eta_{ei} \cdot (1 - d_r)^i \quad (42)$$

where i indicates the year, and for each year E_i is the total electrical energy output (kWh), H_i is the incident solar irradiation, $\tau \cdot \alpha$ is the product of the transmittance of the glazing and the absorbance of the photovoltaic coating η_{ei} is the electrical efficiency (*dimensionless*), and d_r is the (constant) annual degradation rate.

The Evans equation [67] gives the electrical efficiency η_e of a PV module as a function of its temperature and the incident solar irradiance on it:

$$\eta_e = \eta_{ref} \cdot [1 - \beta_{ref} \cdot (T_c - T_{ref})] \quad (43)$$

in this formula, T_c is the PV module temperature at an operating point ($^{\circ}\text{C}$), η_{ref} is the electrical efficiency of the reference operating point, β_{ref} is the temperature coefficient ($1/^{\circ}\text{C}$) and T_{ref} is the PV module temperature of the reference operating point (25°C). The parameters η_{ref} and β_{ref} , are given in the datasheet of the PV module. Although there are several models [68] to determine the T_c , the one presented by Mattei et al. is widely used due to its reliability:

$$T_c = T_a + (NOCT - 20) \cdot \frac{I_t}{800} \quad (44)$$

where T_a is the ambient temperature ($^{\circ}\text{C}$), $NOCT$ is the normal operating cell temperature ($^{\circ}\text{C}$), and I_t is the solar irradiance (W/m^2). The $NOCT$ is determined under the following operating conditions: $I_t = 800$ (W/m^2), $T_a = 20$ ($^{\circ}\text{C}$), and 1 (m/s) wind speed at PV module level.

To facilitate the comparison of different PV mounting systems, solar tracking systems, etc., the term “ $LCOE$ efficiency” is used in the literature [14,19,69]. In this study, we compute the $LCOE$ efficiency as the ratio between the $LCOE$ of a PV system with the optimal deployment ($LCOE_{(\gamma_{opt}, \alpha_{opt})}$) and the $LCOE$ of a south-facing PV system ($LCOE_{(0, \alpha_{opt})}$):

$$\eta_{LCOE} = \frac{LCOE_{(\gamma_{opt}, \alpha_{opt})}}{LCOE_{(0, \alpha_{opt})}} \quad (45)$$

Thus, $\eta_{LCOE} > 1$ means that a system deployed using the optimal configuration in this paper is less efficient than a south-facing one. However, it is necessary to notice the following:

- (i) The number of PV modules per solar tracker is 58, which is the usual one for this type of tracker [7].
- (ii) The initial investment cost is per solar tracker.
- (iii) The discount rates are country specific, therefore only PV systems with the same location will be compared.
- (iv) As the PV system is exposed to the same weather conditions, regardless of its deployment, the parameter d does not depend on the location.

4.3. Weather conditions

Not only the terrain location, but also the meteorological conditions have enormous effect on the optimal deployment of solar trackers. In the case of solar trackers, the weather conditions can be gathered in a single factor: the cloudiness index.

The cloudiness index (or horizontal diffuse fraction or cloud ratio or diffuse ratio) (k_d) is the ratio between the diffuse solar irradiance on horizontal terrain (I_{dh}), and the global solar irradiance on horizontal terrain (I_{gh}) [23]:

$$k_d = \frac{I_{dh}}{I_{gh}} \quad (46)$$

The index k_d reflects the cloudiness of the sky and/or the turbidity of the atmosphere [70]. Thus, the higher the proportion of the diffuse component in the global solar irradiance, the greater the value of k_d . It is also used to define clear, partially cloudy and cloudy sky conditions [40]: (i) clear sky means $k_d \in (0.00, 0.33]$; (ii) partially cloudy sky means $k_d \in (0.33, 0.8)$; and (iii) cloudy sky means $k_d \in (0.8, 1)$.

5. Results and discussion

The optimal solar tracker layout on a sloping terrain in any orientation and, therefore, the incident solar irradiation on the PV field can be obtained based on the equations derived in Section 3 and their implementation in the *Mathematica*[™] code. To show how difficult it is to optimise the deployment of solar trackers, the influence of certain parameters, including weather, sloping terrain, and terrain location, must be known.

The equations derived above for optimising the deployment of solar trackers on sloping terrain with any orientation were used for several parametric analyses: (i) an analysis of the influence of latitude on the optimal deployment of solar trackers, (ii) an analysis of the influence of site weather conditions on the optimal deployment of solar trackers, (iii) an analysis of the energy gain when optimising the deployment of solar trackers, and (iv) an analysis of the $LCOE$ when optimising the deployment of solar trackers.

As the design of a PV power plant depends on a large number of parameters, the following parameters needed to be constantly considered in order for this paper to focus on the corresponding objectives:

- (i) The shape of the available surface. The design of PV power plants is strongly influenced by the irregular shape of the available land [14]. For this reason, the available land was considered to have a regular shape and, moreover, to be the same for all the locations analysed.
- (ii) The type of solar tracker. As this work focuses on horizontal single-axis trackers, this was the solar tracker used throughout the study.
- (iii) The configuration of the PV modules. Although a horizontal single-axis tracker can support several PV module configurations, such as 1 V, 1H, 2 V and 2H [7], the 1 V configuration is the most commonly used configuration for PV power plants [7]. Therefore, it was the one used in this study.
- (iv) The type of PV module. A large number of commercial PV modules are currently available. For example, Belsky et al. [41] analysed 1300 commercial PV modules. Only one commercial PV module was considered in this research work, as extending the analysis to more commercial PV modules would not provide any new conclusions. Any other chosen commercial PV modules could also be implemented in the *Mathematica*™ software code developed. The PV module chosen was the LR5-72HBD 535, a monocrystalline module with 144 cells (6 × 24) by LONGI [71]. The characteristics of the module are: 535 (Wp); dimensions: 1133 × 2256 (mm).
- (v) The limited range of motion angle. In this study, a $\beta_{\max} = \pm 60$ (°) was used, which is the usual value in PV power plants [7].
- (vi) The transverse installation distance. The transverse installation distance is imposed by the clamps used for fastening the PV modules. This distance for the selected model is 25 (mm).
- (vii) The albedo. The albedo depends on several factors such as [72]: the type and roughness of the terrain, the spacing between rows of PV modules, etc. The albedo in this study was considered to be constant with a value of 0.2 [60].
- (viii) The sloping terrain parameters. Sloping terrain is classified according to its aspect [73]. The aspect is defined by the azimuth angle of the sloped terrain (γ_g) and the tilt angle of the terrain (α_g). Fig. 16 shows the range of variation of γ_g and α_g . The range of variation of γ_g is ± 45 (°) (see Fig. 16a). Note that only an analyse from 0 to 45 (°) is necessary since there is symmetry with respect to the south axis. The range of variation of α_g is from 0 to 15 (°) (see Fig. 16b).

Several specific codes were implemented with *Mathematica*™ software for a detailed analysis of the optimisation of horizontal single-axis tracker deployment on sloping terrain with any orientation. These *Mathematica*™ software codes use the equations deduced.

5.1. Case study

The proposed methodology was applied to different locations in order to compare it to the south-facing deployment of the same system. The locations were chosen on the basis of the following criteria:

- (i) The locations under study are in the northern hemisphere. According to a UN report [74], this hemisphere contains approximately 90% of the world's population.
- (ii) All selected locations must be close to the infrastructure necessary for the installation of a PV power plant.
- (iii) The selected locations should have different altitudes in order to ensure a greater difference in weather conditions. Ten locations were chosen using this criterion, ranging from 6 (°) to 60 (°) north

Table 8
Locations under study.

	Locations	Latitude	Longitude	Altitude
1	Medellin (Colombia)	06°14'38" N	75°34'04" W	1469 (m)
2	Bangkok (Thailand)	13°45'14" N	100°29'34" E	9 (m)
3	Morelia (Mexico)	19°42'10" N	101°11'24" W	1921 (m)
4	Karachi (Pakistan)	24°52'01" N	67°01'51" E	14 (m)
5	Cairo (Egypt)	30°29'24" N	31°14'38" W	41 (m)
6	Almeria (Spain)	36°50'07" N	02°24'08" W	22 (m)
7	Toronto (Canada)	43°39'14" N	79°23'13" W	106 (m)
8	Wien (Austria)	48°15'00" N	16°21'00" E	203 (m)
9	Hamburg (Germany)	53°33'00" N	10°00'03" E	19 (m)
10	Helsinki (Finland)	60°10'10" N	24°56'07" E	23 (m)

latitude. These locations have a latitude difference of approximately 6 (°). Their main geographical characteristics are shown in Table 8.

- (iv) The selected locations must be included in the PVGIS database [55]. If the location is not included, determining the incident solar irradiance on the PV field is not possible. Therefore, this criterion is not optional.

The PVGIS database [55] was used to estimate the monthly averages of: (i) beam solar irradiation over horizontal surface, (ii) diffuse solar irradiation over horizontal surface, and (iii) ambient temperature. Fig. 17. shows the ambient conditions at the different locations under study.

A *Mathematica*™ software code was also implemented to calculate the incident solar irradiance on the PV field using the procedure presented in [52].

5.2. Analysis of the influence of latitude on the azimuth angle of solar tracker (γ)

Fig. 18 shows the solar tracker azimuth angle trends for optimal deployment.

The following conclusions can be drawn from Fig. 18:

- (i) The greater the slope angle of the terrain (α_g), the greater the effect of the azimuth angle of the terrain (γ_g) on the optimal azimuth angle of the solar tracker (γ). The optimal azimuth angle of the solar tracker moves away from the south orientation ($\gamma = 0$ (°)) as the slope angle of the terrain increases.
- (ii) The slope of the curve representing the optimal azimuth angle of the solar tracker increases as the latitude of the location of the PV system increases. In other words, the higher the latitude of the location, the further the optimal azimuth angle moves away from the southern orientation ($\gamma = 0$ (°)).
- (iii) The variation of the optimal azimuth angle of the solar tracker is very low for PV system location latitudes between 6 (°) and 19 (°), as it does not exceed 2.5 (°) with respect to the south orientation. In contrast, the variation of the optimal azimuth angle of the solar tracker is remarkable for latitudes above 43 (°) as it is higher than 10 (°). And for intermediate latitudes, between 24 (°) and 36 (°), the variation of the optimal azimuth angle of the solar tracker is between 2.5 (°) and 10 (°). This last case is quite interesting as these locations receive high amounts of solar irradiance.
- (iv) It may be concluded that the deployment of PV systems located at high latitudes is strongly affected by the azimuth angle of the terrain, as the optimal azimuth angle of the solar tracker is significantly away from the southern orientation ($\gamma = 0$ (°)). In contrast, at low latitude locations, the azimuth angle of the terrain has little influence on the optimal azimuth angle of the solar tracker.

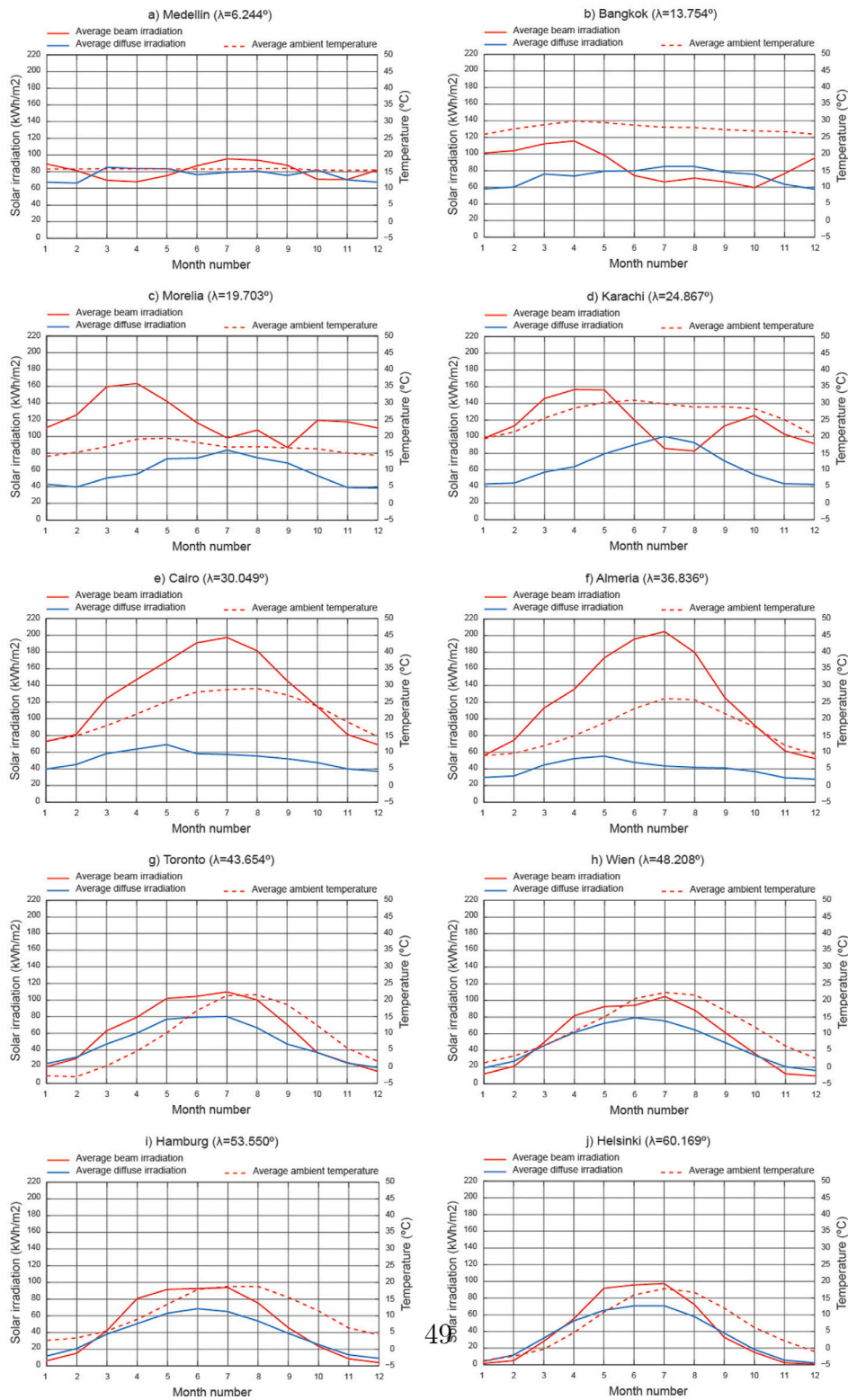


Fig. 17. Environmental conditions.

5.3. Analysis of the influence of site weather conditions on the azimuth angle of solar tracker (γ)

In this section we analyse the influence of meteorological conditions on the optimal deployment of solar trackers using the cloudiness index.

Pairs of locations with the same latitude and different meteorological conditions shall be chosen. It is important to note that it is not

always possible to identify two locations that have the same latitude and have the necessary infrastructure for the installation of a PV power plant due to weather conditions. This is the case in many areas above the 60 (°) parallel in the northern hemisphere that are uninhabited and therefore considered ineligible for this work. The latitude range studied is from 30°N to 43°N. Six locations in five countries were chosen according to this criterion. Table 9 shows the specifications of

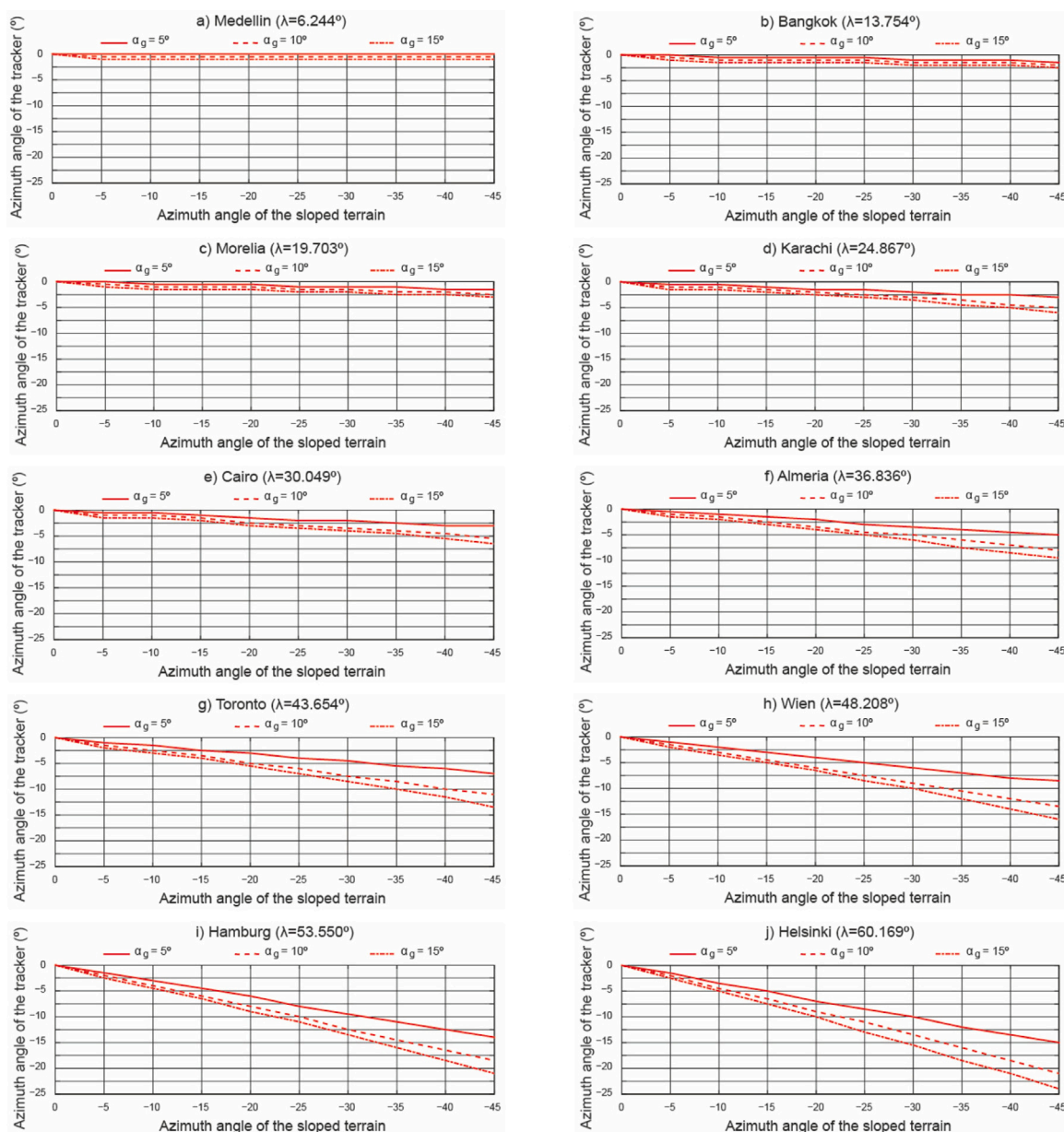


Fig. 18. The influence of latitude and azimuth angle of terrain on the azimuth angle of trackers.

Table 9
Specifications of the sites assessed in terms of weather parameters.

Specifications	Location					
	Comparison 1st		Comparison 2nd		Comparison 3rd	
	Cairo	Chengdu	Almeria	Handan	Toronto	Nice
Latitude	30°29'24" N	30°00'00" N	36°50'07" N	36°36'42" N	43°39'14" N	43°42'11" N
Longitude	31°14'38" W	104°00'00" W	2°24'08" W	114°29'22" E	79°23'13" W	7°15'57" W
Altitude (m)	41	453	22	66	106	18
Annual k_d	0.295	0.679	0.267	0.527	0.462	0.348

the sites assessed according to this criterion. Two locations were studied for the first comparison, Cairo (Egypt) and Chendu (China). Clear sky days predominate in the first location whereas, partially cloudy sky days predominate in the second. The same happens with the second comparison, in this case with Almeria (Spain) and Handan (China). On the other hand, the locations Nice (France) and Toronto (Canada) were studied for the third comparison, where partial sky days predominate

in both locations. Fig. 19 shows the monthly cloudiness index for the locations under study.

Fig. 20 shows the influence of site weather conditions on the azimuth angle of a solar tracker.

The following conclusions can be drawn from Fig. 20:

- (i) In the first comparison, where the PV systems are located at a latitude of 30 (°), there is hardly any difference in the azimuth

Table 10
Standards used for structural calculations.

	Locations	Wind load	Snow load
1	Medellin (Colombia)	NSR-10- Titulo B- cargas [75] ASCE_7-05 [76]	-
2	Bangkok (Thailand)	DPT Standard 1311-50 [77]	-
3	Morelia (Mexico)	CFE-2008_Viento [78] ASCE_7-05 [76]	-
4	Karachi (Pakistan)	BCP SP-2007 [79]	BCP SP-2007 [79]
5	Cairo (Egypt)	ECP-201 [80]	-
6	Almeria (Spain)	CTE DB SE-AE [81] EN 1991-1-4 [82]	CTE DB SE-AE [81] EN 1991-1-3 [82]
7	Toronto (Canada)	NBC 2020 8 [83]	NBC 2020 8 [83]
8	Wien (Austria)	ÖNORM B 1991-1-4:2023-04 [84] EN 1991-1-4 [82]	EN 1991-1-3 [82]
9	Hamburg (Germany)	DIN EN 1991-1-4 [85]	DIN EN 1991-1-3 [86]
10	Helsinki (Finland)	SFS EN 1991-1-4 [87]	SFS EN 1991-1-3 [88]

Table 11
Material and dimensions of profiles used.

Element	Length (mm)	Material	Unit
Central pillar	2440	S 280GD Z275	1
Pillar	2825	S 280GD Z275	8
Central shaft	9900	S 280GD Z275	2
Intermediate shaft 1	8000	S 280GD Z275	2
Intermediate shaft 2	8000	S 280GD Z275	2
Extreme shaft	7800	S 280GD Z275	2
Purlins 1	430	S 280GD Z275	58
Purlins 2	1430	S 280GD Z275	2

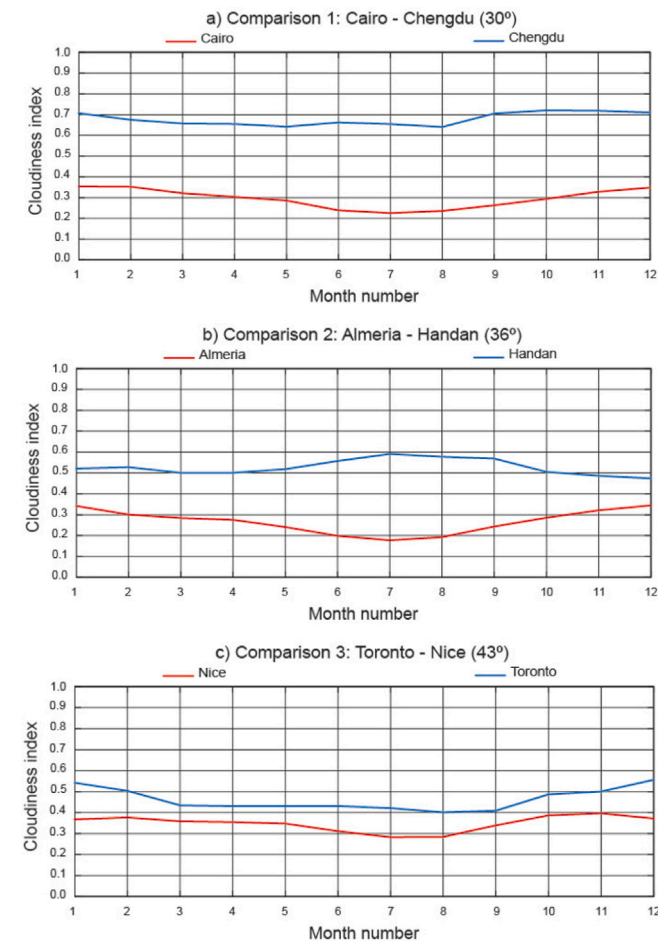


Fig. 19. Monthly cloudiness index for the locations under study.

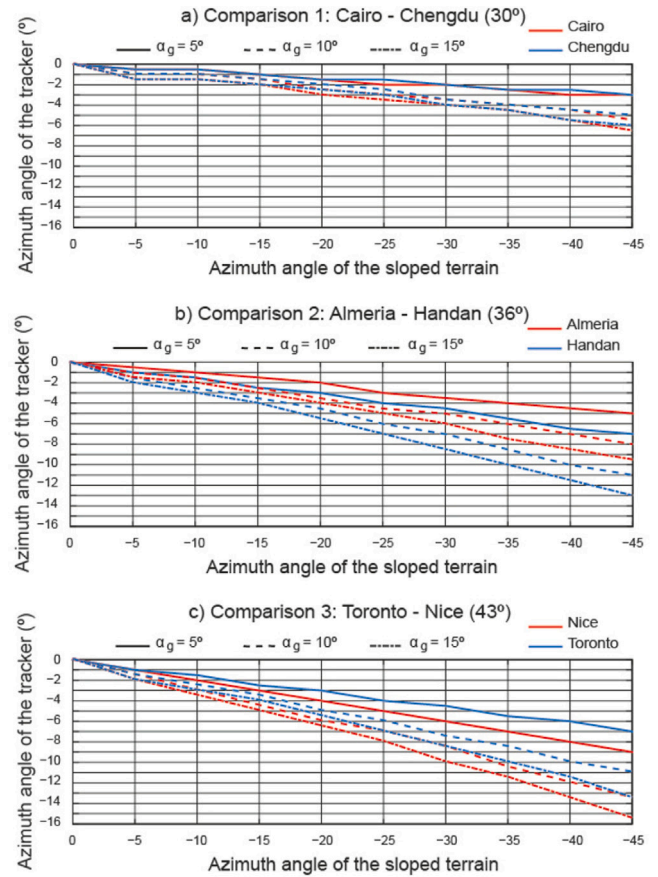


Fig. 20. The influence of site weather conditions on the azimuth angle of a solar tracker.

angle of the solar trackers between the two locations due to the site weather conditions. This is true for all three terrain tilt angles studied. Specifically, the difference in the optimal azimuth angle of the solar tracker of the two locations is at most 0.5 (°). However, for most of the azimuth angles of the terrain, this difference is 0 (°).

- (ii) In the second comparison, where the PV systems are located at a latitude of 36 (°), the site weather conditions affect the choice of the azimuth angle of the solar trackers. The azimuth angle of the solar tracker at the lower k_d location is closer to the south orientation. In addition, the slope angle of the terrain also affects the deployment of the solar trackers. For example, the difference between the optimal azimuth angle of the solar tracker of the two

Table 12
Cost, weight and geometric properties of the profiles used at the Medellín location.

α_g (°)	Central pillar	Pillar	Central shaft	Interm. shaft 1	Interm. shaft 2	Extr. shaft	Purlins 1&2	Weight (kg)	Cost (€)
0	W8 × 13	C195 × 90 × 30 × 3.5	130 × 3.5	130 × 3	130 × 2.5	130 × 2.3	40 × 50 × 25.1 × 1.5	1107.53	1591.33
5	W8 × 13	C195 × 90 × 30 × 3.5	130 × 3.5	130 × 3	130 × 2.5	130 × 2.3	40 × 50 × 25.1 × 1.5	1107.53	1591.33
10	W8 × 13	C195 × 90 × 30 × 3.5	130 × 3.5	130 × 3	130 × 2.5	130 × 2.3	40 × 50 × 25.1 × 1.5	1107.53	1591.33
15	W8 × 13	C195 × 90 × 30 × 3.5	130 × 4.5	130 × 3.5	130 × 3	130 × 2.3	40 × 50 × 25.1 × 1.5	1279.44	1840.15

Table 13
Cost, weight and geometric properties of the profiles used at the Bangkok location.

α_g (°)	Central pillar	Pillar	Central shaft	Interm. shaft 1	Interm. shaft 2	Extr. shaft	Purlins 1&2	Weight (kg)	Cost (€)
0	W8 × 13	C195 × 90 × 30 × 3	130 × 3	130 × 2.5	130 × 2.5	130 × 2.3	40 × 50 × 25.1 × 1.3	983.75	1343.97
5	W8 × 13	C195 × 90 × 30 × 3	130 × 3	130 × 2.5	130 × 2.3	130 × 2.3	40 × 50 × 25.1 × 1.3	983.75	1343.97
10	W8 × 13	C195 × 90 × 30 × 3	130 × 3	130 × 2.5	130 × 2.3	130 × 2.3	40 × 50 × 25.1 × 1.3	983.75	1343.97
15	W8 × 13	C195 × 90 × 30 × 3	130 × 3	130 × 2.5	130 × 2.3	130 × 2.3	40 × 50 × 25.1 × 1.3	983.75	1343.97

Table 14
Cost, weight and geometric properties of the profiles used at the Morelia location.

α_g (°)	Central pillar	Pillar	Central shaft	Interm. shaft 1	Interm. shaft 2	Extr. shaft	Purlins 1&2	Weight (kg)	Cost (€)
0	W8 × 15	C200 × 100 × 30 × 3.5	130 × 4	130 × 3.5	130 × 3.5	130 × 2.3	40 × 50 × 25.1 × 1.5	1265.32	1820.39
5	W8 × 15	C200 × 100 × 30 × 3.5	130 × 4	130 × 3.5	130 × 3.5	130 × 2.3	40 × 50 × 25.1 × 1.5	1265.32	1820.39
10	W8 × 15	C200 × 100 × 30 × 3.5	130 × 4	130 × 3.5	130 × 3.5	130 × 2.3	40 × 50 × 25.1 × 1.5	1265.32	1820.39
15	W8 × 18	C200 × 100 × 40 × 4	130 × 5	130 × 4.5	130 × 3.5	130 × 2.3	40 × 50 × 25.1 × 1.8	1495.02	2286.10

Table 15
Cost, weight and geometric properties of the profiles used at the Karachi location.

α_g (°)	Central pillar	Pillar	Central shaft	Interm. shaft 1	Interm. shaft 2	Extr. shaft	Purlins 1&2	Weight (kg)	Cost (€)
0	W8 × 18	C200 × 100 × 40 × 4	130 × 5	130 × 4	130 × 3.5	130 × 2.3	40 × 50 × 25.1 × 1.8	1482.98	2177.36
5	W8 × 18	C200 × 100 × 40 × 4	130 × 5	130 × 4	130 × 3.5	130 × 2.3	40 × 50 × 25.1 × 1.8	1482.98	2177.36
10	W8 × 18	C200 × 100 × 40 × 4	130 × 5	130 × 4	130 × 3.5	130 × 2.3	40 × 50 × 25.1 × 1.8	1482.98	2177.36
15	W8 × 18	C200 × 100 × 40 × 4	130 × 5	130 × 4	130 × 3.5	130 × 2.3	40 × 50 × 25.1 × 1.8	1482.98	2177.36

locations is at most 3.5 (°) when the azimuth angle of the terrain is 45 (°) and the tilt angle of the terrain is 15 (°).

- (iii) In the third comparison, where the *PV* systems are located at a latitude of 43 (°), the site weather conditions affect the choice of the azimuth angle of the solar tracker. The azimuth angle of the solar tracker at the higher k_d location is closer to the south orientation. In addition, the slope angle of the terrain also affects the deployment of the solar trackers. For example, the difference of the optimal azimuth angle of the solar tracker of the two locations is at most 2.5 (°) when the azimuth angle of the terrain is 45 (°) and the tilt angle of the terrain is 15 (°).
- (iv) It may be concluded that, if the site latitude is constant, the choice of the azimuth angle for the *PV* system, is affected by the weather conditions, the distribution of k_d throughout the year, the azimuth angle of the terrain, and the tilt angle of the terrain. This shows how k_d influences equation (37), which is the one used to maximise the incident solar irradiance on the *PV* field at each location.

5.4. Analysis of the energy gain when optimising the deployment of solar trackers

We use the Energy Gain as an indicator of the value of our methods, via Eq. (39). Fig. 21 shows the influence of latitude on the *EG* at the sites studied.

The following conclusions can be drawn from Fig. 21:

- (i) Using the optimal deployment for *PV* system location latitudes between 6 (°) and 19 (°) does not achieve noticeably better results than using a *PV* system deployment in the a southerly direction.

- (ii) The *EG* is noticeable for *PV* system location latitudes above 19 (°). The following holds true: (a) The higher the location latitude, the higher the *EG*. For example, the *EG* for a terrain tilt angle of 5 (°) and a terrain azimuth angle of 20 (°) in Almeria is 240 (Wh/m²), and for the same parameters in Helsinki it is 390 (Wh/m²); (b) The higher the azimuth angle of the terrain, the higher the *EG*. For example, in Almeria the *EG* for a terrain tilt angle of 5 (°) and a terrain azimuth angle of 20 (°) is 240 (Wh/m²), and 530 (Wh/m²) for a terrain azimuth angle of 30 (°); and (c) The higher the tilt angle of the terrain, the higher the *EG*. For example, in Almeria the *EG* for a terrain azimuth angle of 20 (°) and a terrain tilt angle of 5 (°) is 240 (Wh/m²), and 1030 (Wh/m²) for a terrain tilt angle of 15 (°).
- (iii) It may be concluded that the deployment of *PV* systems in mid and high latitudes is strongly affected by the procedure used for their calculation. Notice the remarkable high value of the solar irradiance on mid-latitudes. In contrast, the procedure used to deploy the *PV* system has no influence at low latitude locations.

5.5. LCOE efficiency

Eq. (45) is used to determine the *LCOE* efficiency at each location. It requires knowledge of: (i) the net project cost, and (ii) the energy generated by the *PV* system over its lifetime. We studied in Section 4 all the relevant details.

We have included, in Annex B, a list of the results of the structural analysis carried out with the AutoDesk Robot software. Table 11 contains the material and dimensions of the profiles used. Tables 12–21 show the geometrical properties, weight and cost of the profiles calculated, respectively, for Medellín, Bangkok, Morelia, Karachi, Cairo,

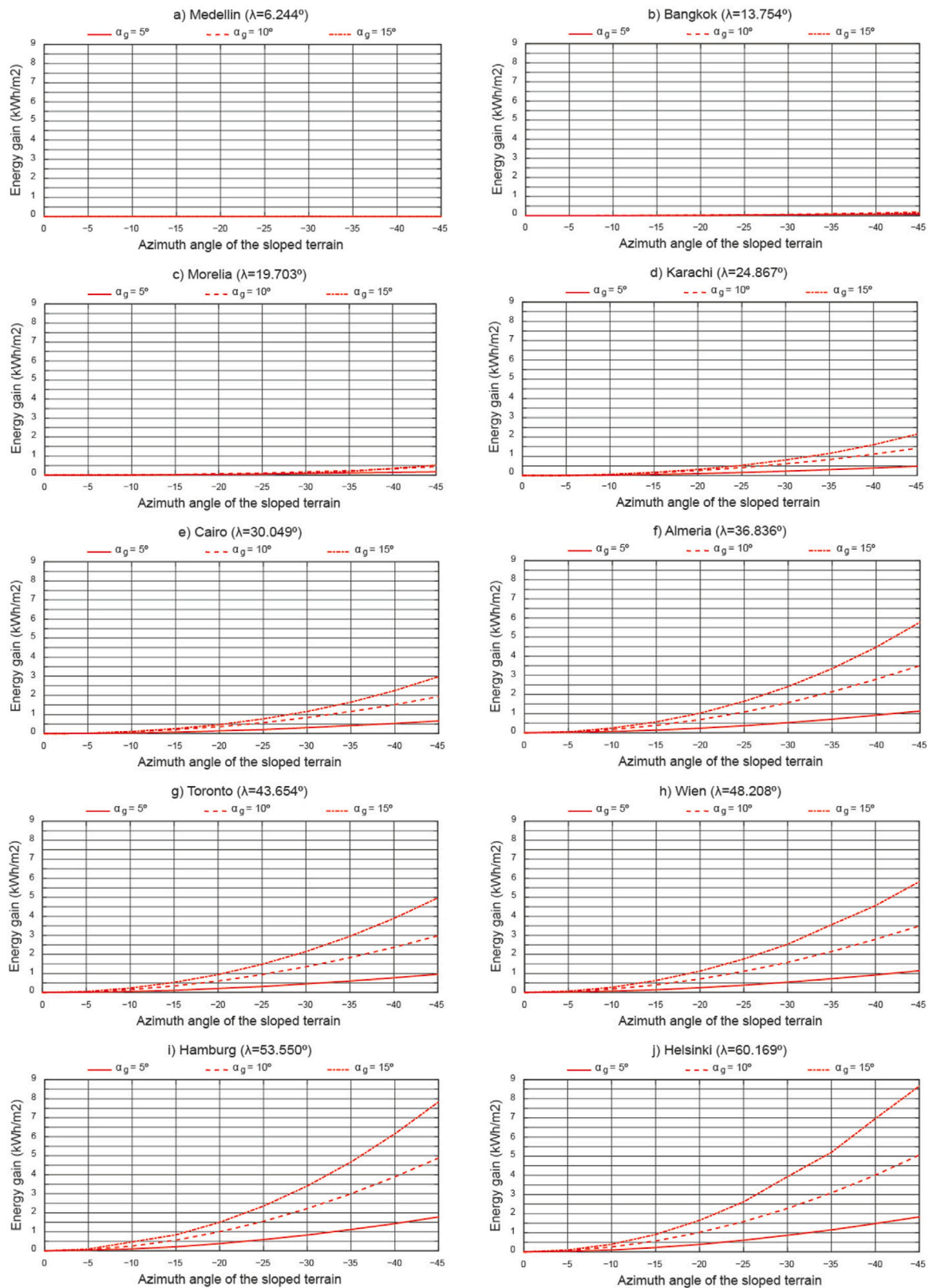


Fig. 21. The influence of latitude and the azimuth angle of terrain on EG.

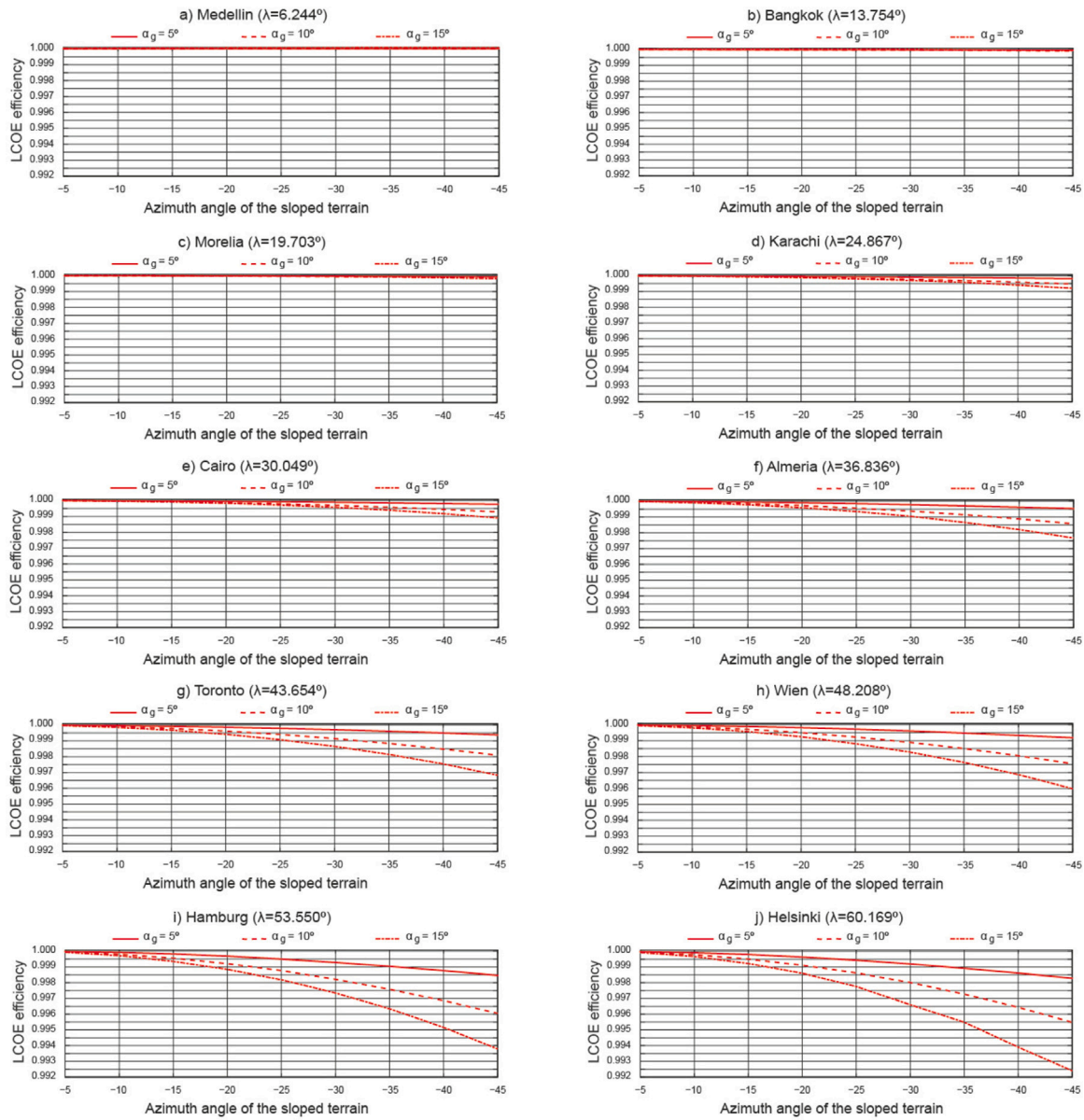


Fig. 22. The influence of the azimuth angle and tilt angle of the terrain on the LCOE efficiency.

Table 16

Cost, weight and geometric properties of the profiles used at the Cairo location.

α_g (°)	Central pillar	Pillar	Central shaft	Interm. shaft 1	Interm. shaft 2	Extr. shaft	Purlins 1&2	Weight (kg)	Cost (€)
0	W8 × 15	C195 × 90 × 30 × 4	130 × 4.5	130 × 3.5	130 × 3	130 × 2.3	40 × 50 × 25.1 × 1.5	1322.60	1915.45
5	W8 × 18	C200 × 100 × 30 × 4	130 × 5	130 × 4	130 × 3.5	130 × 2.3	40 × 50 × 25.1 × 1.6	1460.28	2126.98
10	W8 × 18	C200 × 100 × 40 × 4	130 × 5	130 × 4.5	130 × 4	130 × 2.3	40 × 50 × 25.1 × 1.6	1536.52	2253.10
15	W8 × 21	C200 × 100 × 40 × 4	130 × 5	130 × 5	130 × 4.5	130 × 2.3	40 × 50 × 25.1 × 1.8	1693.96	2486.48

Table 17

Cost, weight and geometric properties of the profiles used at the Almeria location.

α_g (°)	Central pillar	Pillar	Central shaft	Interm. shaft 1	Interm. shaft 2	Extr. shaft	Purlins 1&2	Weight (kg)	Cost (€)
0	W8 × 13	C195 × 90 × 30 × 3.5	130 × 2.5	130 × 2.5	130 × 2.5	130 × 2.3	40 × 50 × 25.1 × 1.5	1037.47	1500.38
5	W8 × 15	C195 × 90 × 30 × 4	130 × 3	130 × 2.5	130 × 2.5	130 × 2.3	40 × 50 × 25.1 × 1.5	1119.88	1625.43
10	W8 × 18	C200 × 100 × 30 × 4	130 × 3	130 × 3	130 × 3	130 × 2.3	40 × 50 × 25.1 × 1.5	1211.74	1747.27
15	W8 × 18	C200 × 100 × 40 × 4	130 × 3	130 × 3	130 × 3	130 × 2.3	40 × 50 × 25.1 × 1.6	1230.24	1790.48

Almeria, Toronto, Wien, Hamburg and Helsinki. All the data used for preparing these cost studies refer to 06/11/2024.

Annex C lists the costs of the PV modules, the control system and the motor (see Table 22), as of 06/11/2024.

Table 18
Cost, weight and geometric properties of the profiles used at the Toronto location.

α_g (°)	Central pillar	Pillar	Central shaft	Interm. shaft 1	Interm. shaft 2	Extr. shaft	Purlins 1&2	Weight (kg)	Cost (€)
0	W8 × 13	C195 × 90 × 30 × 3	130 × 3	130 × 3	130 × 2.3	130 × 2.3	40 × 50 × 25.1 × 1.3	1040.16	1484.89
5	W8 × 13	C195 × 90 × 30 × 3	130 × 3	130 × 3	130 × 2.3	130 × 2.3	40 × 50 × 25.1 × 1.3	1040.16	1484.89
10	W8 × 13	C195 × 90 × 30 × 3	130 × 3	130 × 3	130 × 2.3	130 × 2.3	40 × 50 × 25.1 × 1.3	1040.16	1484.89
15	W8 × 13	C195 × 90 × 30 × 3	130 × 3.5	130 × 3	130 × 2.3	130 × 2.3	40 × 50 × 25.1 × 1.5	1107.53	1591.33

Table 19
Cost, weight and geometric properties of the profiles used at the Wien location.

α_g (°)	Central pillar	Pillar	Central shaft	Interm. shaft 1	Interm. shaft 2	Extr. shaft	Purlins 1&2	Weight (kg)	Cost (€)
0	W8 × 10	C195 × 90 × 30 × 3	130 × 2.3	130 × 2.3	130 × 2.3	130 × 2.3	40 × 50 × 25.1 × 1.5	960.82	1385.62
5	W8 × 13	C195 × 90 × 30 × 3	130 × 2.3	130 × 2.3	130 × 2.3	130 × 2.3	40 × 50 × 25.1 × 1.5	1068.34	1560.43
10	W8 × 13	C195 × 90 × 30 × 3.5	130 × 2.3	130 × 2.3	130 × 2.3	130 × 2.3	40 × 50 × 25.1 × 1.5	1211.74	1747.27
15	W8 × 13	C195 × 90 × 30 × 3.5	130 × 2.3	130 × 2.3	130 × 2.3	130 × 2.3	40 × 50 × 25.1 × 1.6	1215.43	1750.88

Table 20
Cost, weight and geometric properties of the profiles used at the Hamburg location.

α_g (°)	Central pillar	Pillar	Central shaft	Interm. shaft 1	Interm. shaft 2	Extr. shaft	Purlins 1&2	Weight (kg)	Cost (€)
0	W8 × 13	C195 × 90 × 30 × 3.5	130 × 2.3	130 × 2.3	130 × 2.3	130 × 2.3	40 × 50 × 25.1 × 1.5	960.82	1385.62
5	W8 × 15	C195 × 90 × 30 × 4	130 × 2.5	130 × 2.5	130 × 2.3	130 × 2.3	40 × 50 × 25.1 × 1.5	1068.34	1560.43
10	W8 × 18	C195 × 100 × 30 × 4	130 × 3	130 × 3	130 × 3	130 × 2.3	40 × 50 × 25.1 × 1.5	1211.74	1747.28
15	W8 × 18	C195 × 100 × 30 × 4	130 × 3	130 × 3	130 × 3	130 × 3.3	40 × 50 × 25.1 × 1.6	1215.43	1750.88

Table 21
Cost, weight and geometric properties of the profiles used at the Helsinki location.

α_g (°)	Central pillar	Pillar	Central shaft	Interm. shaft 1	Interm. shaft 2	Extr. shaft	Purlins 1&2	Weight (kg)	Cost (€)
0	W8 × 10	C195 × 90 × 30 × 3	130 × 2.3	130 × 2.3	130 × 2.3	130 × 2.3	40 × 50 × 25.1 × 1.3	941.56	1360.68
5	W8 × 13	C195 × 90 × 30 × 3	130 × 2.3	130 × 2.3	130 × 2.3	130 × 2.3	40 × 50 × 25.1 × 1.3	960.60	1395.76
10	W8 × 13	C195 × 100 × 30 × 3.5	130 × 2.3	130 × 2.3	130 × 2.3	130 × 2.3	40 × 50 × 25.1 × 1.5	1004.50	1459.51
15	W8 × 13	C195 × 100 × 30 × 3.5	130 × 2.3	130 × 2.3	130 × 2.3	130 × 2.3	40 × 50 × 25.1 × 1.5	1004.50	1459.51

Annex D covers the cost of auxiliary components of the photovoltaic mounting system (see Table 23), as of 06/11/2024.

Eq. (42) determines the energy generated by the PV system over its lifetime. It uses (i) Eq. (36) to calculate the incident energy, (ii) Eq. (44) to determine the temperature of the modules temperature, and (iii) Eq. (43) to determine their electrical efficiency

Fig. 22 shows the influence of the azimuth angle and tilt angle of the terrain on the LCOE efficiency. The following conclusions can be drawn from Fig. 22:

- (i) For latitudes between 6 (°) and 19 (°), the LCOE of the optimal configuration is essentially the same as for south-facing systems.
- (ii) For latitudes higher than 19 (°) the following holds: (a) The higher the latitude of the site, the higher the LCOE of the optimal configuration. For instance, the LCOE efficiency for a terrain tilt angle of 5 (°) and a terrain azimuth angle of 20 (°) in Almeria is 0.99990, and for the same parameters in Helsinki it is 0.99963; (b) The higher the azimuthal terrain angle, the higher the LCOE obtained when using the optimal deployment of solar trackers. For example, in Almeria the LCOE efficiency for a terrain tilt angle of 5 (°) and a terrain azimuthal angle of 20 (°) is 0.99990, and 0.99977 for a terrain azimuthal angle of 30 (°); and (c) The higher the terrain tilt angle, the higher the LCOE of the optimal deployment. For example, in Almeria the LCOE efficiency for a terrain azimuth angle of 20 (°) and a terrain tilt angle of 5 (°) is 0.99990, and 0.99959 for a terrain tilt angle of 15 (°).
- (iii) Thus, the optimal deployment of solar trackers in PV systems at mid and high latitudes obtains higher LCOE. The fact that large amounts of solar irradiation are received at mid-latitudes

must be taken into account. In contrast, the difference between the south-oriented and the optimal PV system is essentially nil.

6. Conclusions

This paper describes a methodology for optimising the deployment of horizontal single-axis trackers on terrain with arbitrary orientation and slope. This is a complex problem, as it involves at least 14 relevant parameters. Our aim is to optimise the azimuth and tilt angles of the solar tracker for each given location, taking into account the meteorological conditions, and the azimuth tilt angles of the terrain. The steps of our method are: (i) Deduction of the coordinate system, (ii) Deduction of the relation between the angles of the terrain (α_g and γ_g) and the angles of the solar tracker (α and γ), (iii) Transformation of the reference system S' into the system S'' , (iv) Choice of the inter-row spacing (in the new reference system S''), (v) Computation of the operating periods and motion of the solar tracker (in the new reference system S''), (vi) Optimization of the position of the solar trackers, and (vii) Validation. Three evaluation indicators (weather conditions at the site, Energy gain, LCOE efficiency) were analysed for azimuth angles of the terrain between 0 (°) and ± 45 (°), and terrain tilt angles between 0 (°) and 15 (°) at 10 locations in the Northern Hemisphere. The following main conclusions can be highlighted:

- (i) The robustness of the derived equations was demonstrated by validating them from three perspectives: numerical validation, validation using PVsyst software and experimental validation.
- (ii) The azimuth angle of a PV system located at high latitudes is strongly affected by the azimuth angle of the terrain. In contrast,

Table 22
Costs of the PV modules, control system and motor.

Element	Units	Total cost (€)
PV module model (LR5-72HBD 535 (LONGI))	58	9610.02
Slewdrive (motor)	1	437.80
TCU (Tracker Control Unit)	1	108.95

at low latitude locations, the azimuth angle of the terrain has very little influence on the azimuth angle of a solar tracker.

- (iii) If the site latitude is constant, the azimuth angle of a PV system, is affected by the weather conditions, the distribution of k_d throughout the year, the azimuth angle of the terrain and the tilt angle of the terrain.
- (iv) For PV system site latitudes between 6 (°) and 19 (°), the optimal deployment does not achieve significantly better results than deploying a PV system in a southerly direction. In contrast, the energy gain (EG) is significant if this comparison is made at locations with latitudes above 19 (°): (a) The higher the location latitude, the higher the EG. For example, in Almeria the EG for a terrain tilt angle of 5 (°) and a terrain azimuth angle of 20 (°) is 240 (Wh/m²), and 390 (Wh/m²) for the same parameters in Helsinki; (b) The higher the azimuth angle of the terrain, the higher the EG. For example, in Almeria the EG for a terrain tilt angle of 5 (°) and a terrain azimuth angle of 20 (°) is 240 (Wh/m²), and 530 (Wh/m²) for a terrain azimuth angle of 30 (°); and (c) The higher the tilt angle of the terrain, the higher the EG. For example, in Almeria the EG for a terrain azimuth angle of 20 (°) and a terrain tilt angle of 5 (°) is 240 (Wh/m²), and 1030 (Wh/m²) for a terrain tilt angle of 15 (°).
- (v) For latitudes between 6 (°) and 19 (°), similar LCOEs are obtained to those provided by southward deployed trackers. For locations with latitudes higher than 19 (°) we have: (a) The higher the latitude of the site, the higher the LCOE obtained when using the optimal deployment of solar trackers; (b) The higher the azimuthal terrain angle, the higher the LCOE obtained when using the optimal deployment; and (c) The higher the terrain tilt angle, the higher the LCOE obtained when using the optimal deployment.

The final conclusion is that the deployment of PV systems at high latitudes is strongly affected by the azimuth angle of the terrain. In contrast, the azimuth angle of the terrain has very little influence at low latitude locations.

An essential aspect of decision-making in photovoltaic projects is the analysis of the economic benefits associated with the deployment of solar trackers in a given location. In our opinion, this study may be of relevance for hybrid wind/photovoltaic power plants.

CRediT authorship contribution statement

A. Barbón: Methodology, Conceptualization. **J. Aparicio-Bermejo:** Writing – original draft, Software, Methodology, Conceptualization. **L. Bayón:** Methodology, Conceptualization. **P. Fortuny Ayuso:** Writing – original draft, Software, Methodology.

Declaration of competing interest

The authors declare that they have no known competing financial interests or personal relationships that could have appeared to influence the work reported in this paper.

Acknowledgements

We wish to thank Gonvarri Solar Steel [7] for their contributions to this study.

Table 23
Costs of the other elements.

Element	Standard	Material	Surface treatam.	Units	Total cost (€)
Joint shafts	–	–	HD G*	6	40.26
Pillar bearing	–	–	HD G*	6	91.74
Motor supp,	–	–	HD G*	1	28.00
Antenna supp,	–	–	HD G*	1	0.87
TCU* supp,	–	–	HD G*	2	10.62
NCU* supp,	–	–	HD G*	2	74.82
NCU* supp,	–	–	HD G*	2	179.58
RCU* supp,	–	–	HD G*	1	217.34
RSU* supp,	–	–	HD G*	1	40.01
Damper	–	–	–	4	140.8
End clamp	DIN 933	Aluminium		8	6.95
Clamp	DIN 933	Aluminium		108	136.62
Screw M16 × 40	DIN 6921 8.8	Class 8.8	HD G	72	11.36
Nut M16	DIN 6923 8	Class 8.8	HD G	72	1.56
Screw M16 × 60	DIN 6921 8.8	Class 8.8	HD G	4	0.68
Nut M16	DIN 6923 8	Class 8.8	HD G	4	0.09
Screw M10 × 55	DIN 6921 8.8 4 7	Class 8.8	HD G	24	0.89
Nut M10	DIN 6923 8 4 8	Class 8.8	HD G	24	0.24
Screw M12 × 30	DIN 6921 8.8 4 9	Class 8.8	HD G	24	2.04
Nut M12	DIN 6923 8	Class 8.8	HD G	24	0.98
Screw M16 × 30	DIN 6921 8.8	Class 8.8	HD G	116	19.43
Square U Bolt	SBS-04 1 7	Class 8.8	HD G	58	33.81
Nut M16	DIN 6923 8	Class 8.8	Stainless	116	2.30

ANNEX A: Standards used for structural calculations

See Table 10.

ANNEX B: Profile properties: material, geometric properties, dimensions, weight and cost

See Tables 11–21.

ANNEX C: Costs of PV modules, control system and motor.

See Table 22.

ANNEX D: Cost of auxiliary components of the photovoltaic mounting system

See Table 23.

Data availability

Data will be made available on request.

References

- [1] Agreement P. Paris agreement. In: Report of the conference of the parties to the United Nations framework convention on climate change (21st session, 2015: Paris). 2015.
- [2] Eurostat. EU overachieves 2020 renewable energy target. 2024, Available from: <https://ec.europa.eu/eurostat/web/products-eurostat-news/-/dn-20220119-1>. [Accessed on 6 March 2024].
- [3] IRENA. World energy transitions outlook 2023: 1.5°C pathway. 2023, International Renewable Energy Agency, Abu Dhabi, Available from: <https://www.irena.org/Publications/2023/Jun/World-Energy-Transitions-Outlook-2023>. [Accessed on 6 March 2024].
- [4] Schyska BU, Kies A, Schlott M, von Bremen L, Medjroubi W. The sensitivity of power system expansion models. *Joule* 2021;5:2606–24.
- [5] International Energy Agency (IEA). World energy outlook 2023. 2024, Available from: <https://iea.blob.core.windows.net/assets/ed1e4c42-5726-4269-b801-97b3d32e117c/WorldEnergyOutlook2023.pdf>. [Accessed on 6 March 2024].

- [6] International Renewable Energy Agency (IRENA). Renewable energy statistics 2023. 2024, Available from: <https://www.irena.org/Publications/2023/Jul/Renewable-energy-statistics-2023>. [Accessed on 6 March 2024].
- [7] Gonvarri solar steel. 2024, Available from: <https://www.gsolarsteel.com/>. [Accessed on 6 March 2024].
- [8] Barbón A, Fortuny Ayuso P, Bayón L, Silva CA. A comparative study between racking systems for photovoltaic power systems. *Renew Energy* 2021;180:424–37.
- [9] Martín-Martínez S, Cañas-Carretón M, Honrubia-Escribano A, Gómez-Lázaro E. Performance evaluation of large solar photovoltaic power plants in Spain. *Energy Convers Manage* 2019;183:515–28.
- [10] Future market insights, solar trackers market: Solar trackers market analysis by single-axis and dual-axis for 2023 to 2033. 2024, Available from: <https://www.futuremarketinsights.com/reports/solar-trackers-market>. [Accessed on 6 March 2024].
- [11] Chunduri SK, Schmela M. Market Survey Solar Trackers 2022, Available from: <https://taiyangnews.info/solar-trackers-market-survey-2022/>.
- [12] Antaisolar. 2024, Available from: <https://www.antisolar.com/>. [Accessed on 6 March 2024].
- [13] Barbón A, Bayón-Cueli C, Bayón L, Carreira-Fontao V. A methodology for an optimal design of ground-mounted photovoltaic power plants. *Appl Energy* 2022;314:118881.
- [14] Barbón A, Carreira-Fontao V, Bayón L, Silva CA. Optimal design and cost analysis of single-axis tracking photovoltaic power plants. *Renew Energy* 2023;211:626–46.
- [15] Tawalbeh M, Al-Othman A, Kafiah F, Abdelsalam E, Almomani F, Alkasrawi M. Environmental impacts of solar photovoltaic systems: A critical review of recent progress and future outlook. *Sci Total Environ* 2021;759:143528.
- [16] Dias L, Gouveia JP, Lourenço P, Seixas J. Interplay between the potential of photovoltaic systems and agricultural land use. *Land Use Policy* 2019;81:725–35.
- [17] Food and Agriculture Organization (FAO). 2024, Available from: <https://databank.worldbank.org/metadataglossary/world-development-indicators/series/AG.LND.AGRI.ZS>. [Accessed on 6 March 2024].
- [18] Barbón A, Rodríguez-Fernández C, Bayón L, Aparicio-Bermejo J. Evaluating the potential of floating photovoltaic plants in pumped hydropower reservoirs in Spain. *Electronics* 2024;13:832.
- [19] Barbón A, Ayuso PFortuny, Bayón L, Silva CA. Experimental and numerical investigation of the influence of terrain slope on the performance of single-axis trackers. *Appl Energy* 2023;348:121524.
- [20] Eurostat. 2024, Available from: https://ec.europa.eu/eurostat/statistics-explained/index.php?title=Agricultural_land_prices_and_rents_statistics&oldid=559924. [Accessed on 6 March 2024].
- [21] Turner R, Newton CM, Dennis DF. Economic relationships between parcel characteristics and price in the market for Vermont forestland. *For Sci* 1991;37:1150–62.
- [22] Zheng N, Tao Y, Sun Y, Zhu J, Yang K, Jiang Z, Dong B, Ren J, Wang Y. A quadratic programming optimization of field leveling for large-scale photovoltaic plant. *Results Phys* 2024;61:107791.
- [23] Duffie JA, Beckman WA. *Solar engineering of thermal processes*. John Wiley & Sons; 2013.
- [24] Gómez-Uceda FJ, Moreno-García IM, Jiménez-Martínez JM, López-Luque R, Fernández-Ahumada LM. Analysis of the influence of terrain orientation on the design of PV facilities with single-axis trackers. *Appl Sci* 2020;10:8531.
- [25] Casares de la Torre FJ, Varo M, López-Luque R, Ramírez-Faz J, Fernández-Ahumada LM. Design and analysis of a tracking / backtracking strategy for PV plants with horizontal trackers after their conversion to agrivoltaic plants. *Renew Energy* 2022;187:537–50.
- [26] Huang B, Huang J, Xing K, Liao L, Xie P, Xiao M, Zhao W. Development of a solar-tracking system for horizontal single-axis PV arrays using spatial projection analysis. *Energies* 2023;16:4008.
- [27] Pierce B, Stein J, Riley D. Single axis tracker performance modeling on sloped terrain. In: *IEEE 50th photovoltaic specialists conference*. 2023, p. 4.
- [28] Bruno R, Bevilacqua P, Longo L, Arcuri N. Small size single-axis PV trackers: control strategies and system layout for energy optimization. *Energy Procedia* 2015;82:737–43.
- [29] Anderson K. Maximizing yield with improved single-axis backtracking on cross-axis slopes. In: *2020 47th IEEE photovoltaic specialists conference. PVSC, 2020*, p. 1466–71.
- [30] Lorenzo E, Narvarte L, Muñoz J. Tracking and back-tracking. *Prog Photovolt, Res Appl* 2011;19:747–53.
- [31] Anderson K, Mikofski M. Slope-aware backtracking for single-axis trackers. No. NREL/TP-5K00-76626, Golden, CO (United States): National Renewable Energy Lab.(NREL); 2020.
- [32] Ledesma JR, Lorenzo E, Narvarte L. Single-axis tracking and bifacial gain on sloping terrain. *Prog Photovolt, Res Appl* 2024;1–17.
- [33] López M. Detection of tracker misalignments and estimation of cross-axis slope in photovoltaic plants. *Sol Energy* 2024;272:112490.
- [34] Aronescu A, Appelbaum J. The effect of collector azimuth on inter-row shading in photovoltaic fields—A comprehensive point of view. *Energies* 2023;16:4876.
- [35] Anderson KS, Jensen AR. Shaded fraction and backtracking in single-axis trackers on rolling terrain. *J Renew Sustain Energy* 2024;16:023504.
- [36] Pvsyst. 2024, Available from: <https://www.pvsyst.com/>. [Accessed on 6 March 2024].
- [37] Solarfarmer. 2024, Available from: <https://solarfarmer.dnv.com/welcome>. [Accessed on 6 March 2024].
- [38] RETScreen. 2024, Available from: <https://natural-resources.canada.ca/maps-tools-and-publications/tools/modelling-tools/retscreen/7465>. [Accessed on 6 March 2024].
- [39] Bayón-Cueli C, Barbón A, Bayón L, Fernández-Conde A. Influence of terrain slope on the performance of single-axis trackers. In: *Proceedings of short papers of the fourth int. scientific conference alternative energy sources, materials & technologies*. 2021, p. 43–4.
- [40] Kong HJ, Kim JT. A classification of real sky conditions for Yongin, Korea. In: *Sustainability in energy and buildings conference*, vol. 22, springer; 2013, p. 1025–32.
- [41] Belsky AA, Glukhanich DY, Carrizosa MJ, Starshaia VV. Analysis of specifications of solar photovoltaic panels. *Renew Sustain Energy Rev* 2022;159:112239.
- [42] IDAE. Technical conditions for PV installations connected to the grid [in Spanish]. Spanish Government Technical Report, Spain: Report Available from the Publication Services of the Institute for Diversification and Energy Savings; 2011, Available from: <http://www.idae.es>. [Accessed on 6 March 2024].
- [43] China federation of power enterprises. Design specification of photovoltaic power station. Beijing: China Planning Press; 2012.
- [44] Martín-Chivelet N. Photovoltaic potential and land-use estimation methodology. *Energy* 2016;94:233–42.
- [45] Montealegre AL, García-Pérez S, Guillén-Lambea S, Monzón-Chavarrías M, Sierra-Pérez J. GIS-based assessment for the potential of implementation of food-energy-water systems on building rooftops at the urban level. *Sci Total Environ* 2022;803:149963.
- [46] Barbón A, Ghodbane M, Bayón L, Said Z. A general algorithm for the optimization of photovoltaic modules layout on irregular rooftop shapes. *J Clean Prod* 2022;365:132774.
- [47] Liu BYH, Jordan RC. The long-term average performance of flat-plate solar energy collectors. *Sol Energy* 1963;7:53–74.
- [48] Makhdoomi S, Askarzadeh A. Impact of solar tracker and energy storage system on sizing of hybrid energy systems: A comparison between diesel/PV/PHS and diesel/PV/fc. *Energy* 2021;231:120920.
- [49] Zhu Y, Liu J, Yang X. Design and performance analysis of a solar tracking system with a novel single-axis tracking structure to maximize energy collection. *Appl Energy* 2020;264:114647.
- [50] Conceicao R, Silva HG, Fialho L, Lopes FM, Collares-Pereira M. PV system design with the effect of soiling on the optimum tilt angle. *Renew Energy* 2019;133:787–96.
- [51] Mehleri ED, Zervas PL, Sarimveis H, Palyvos JA, Markatos NC. Determination of the optimal tilt angle and orientation for solar photovoltaic arrays. *Renew Energy* 2010;35:2468–75.
- [52] Barbón A, Ayuso PFortuny, Bayón L, Fernández-Rubiera JA. Predicting beam and diffuse horizontal irradiance using Fourier expansions. *Renew Energy* 2020;154:46–57.
- [53] Hottel HC. A simple model for estimating the transmittance of direct solar radiation through clear atmosphere. *Sol Energy* 1976;18:129–34.
- [54] Liu BYH, Jordan RC. The interrelationship and characteristic distribution of direct. *Diffus Total Sol Radiat Sol Energy* 1960;4:1–19.
- [55] PVGIS. Joint research centre (JRC). 2020, Available from: http://re.jrc.ec.europa.eu/pvg_tools/en/tools.html. [Accessed 18 January 2024].
- [56] IRENA. Innovation outlook: Renewable mini-grids. International Renewable Energy Agency. 2016, Available from: <https://www.irena.org/publications/2016/Sep/Innovation-Outlook-Renewable-mini-grids>. [Accessed on 6 March 2024].
- [57] Elkadeem MR, Zainali S, Ma Lu S, Younes A, Abido MA, Amaducci S, Croci M, Zhang J, Landelius T, Stridh B, Elia Campana P. Agrivoltaic systems potentials in Sweden: A geospatial-assisted multi-criteria analysis. *Appl Energy* 2024;356:122108.
- [58] Radwan A, Mdallal A, Haridy S, Ali Abdalkareem M, Hai Alami A, Ghani Olabi A. Optimizing the annual energy yield of a residential bifacial photovoltaic system using response surface methodology. *Renew Energy* 2014;222:119914.
- [59] Fan L, Liu C, Dai B, Li J, Wu Z, Guo Y. Electric vehicle routing problem considering energy differences of charging stations. *J Clean Prod* 2023;418:138184.
- [60] Barbón A, Bayón L, Díaz G, Silva CA. Investigation of the effect of albedo in photovoltaic systems for urban applications: Case study for Spain. *Energies* 2022;15:7905.
- [61] Al-Waeli AHA, Chaichan MT, Sopian K, Kazem HA, Mahood HB, Khadom AA. Modeling and experimental validation of a PVT system using nanofluid coolant and nano-PCM. *Sol Energy* 2019;177:178–91.
- [62] Bahrami A, Okoye CO, Atikol U. Technical and economic assessment of fixed, single and dual-axis tracking PV panels in low latitude countries. *Renew Energy* 2017;113:563–79.
- [63] Dukan M, Gut D, Gumber A, Steffen B. Harnessing solar power in the Alps: A study on the financial viability of mountain PV systems. *Appl Energy* 2024;375:124019.

- [64] Branker K, Pathak MJM, Pearce JM. A review of solar photovoltaic leveled cost of electricity. *Renew Sustain Energy Rev* 2011;15:4470–82.
- [65] AutoDesk. Robot structural analysis software. 2024, Available from: <https://www.autodesk.com/products/robot-structural-analysis/overview>. [Accessed 18 July 2024].
- [66] NREL. Best practices for operation and maintenance of photovoltaic and energy storage systems. 3rd ed. Golden, CO: National Renewable Energy Laboratory; 2018, Available from: <https://www.nrel.gov/docs/fy19osti/73822.pdf>. [Accessed 18 July 2024].
- [67] Evans DL. Simplified method for predicting photovoltaic array output. *Sol Energy* 1981;27:555–60.
- [68] Dutra Silva D, Marson V, Rodrigues de Souza R, Diehl de Oliveira J, Campos Silva JB, Cardoso EM. A new predictive model for a photovoltaic module's surface temperature. *Energy Rep* 2022;8:15206–20.
- [69] Boubault A, Ho CK, Hall A, Lambert TN, Ambrosini A. Levelized cost of energy (LCOE) metric to characterize solar absorber coatings for the CSP industry. *Renew Energy* 2016;85:472–83.
- [70] Kambezidis HD. The solar radiation climate of athens: variations and tendencies in the period 1992–2017, the brightening era. *Sol Energy* 2018;173:328–47.
- [71] LONGI. 2024, Available from: <https://www.longi.com/es/products/modules/himo-5/>. [Accessed on 6 March 2024].
- [72] Antonanzas J, Urraca R, Martínez-de Pison FJ, Antonanzas F. Optimal solar tracking strategy to increase irradiance in the plane of array under cloudy conditions: A study across Europe. *Sol Energy* 2018;163:122–30.
- [73] Wang H, Hu G, Ma J, Wei H, Li S, Tang G, Xiong L. Classifying slope unit by combining terrain feature lines based on digital elevation models. *Land* 2023;12:193.
- [74] UN. World population prospects 2022. United Nations. 2022, Available from: <https://population.un.org/wpp/>. [Accessed on 6 March 2024].
- [75] NSR-10- Título B- cargas.
- [76] ASCE 7-05.
- [77] DPT Standard 1311-50.
- [78] CFE-2008_Viento.
- [79] BCP SP-2007.
- [80] ECP-201. Egyptian code of practice for calculation of loads and forces in structures and buildings. 2012, National Housing and Building Research Center, Cairo.
- [81] Spanish technical building code royal decree 314/2006, 17. 2006.
- [82] UNE-EN 1991-1-7: 2018. Actions on structures. AENOR. 2018.
- [83] National building code of Canada: 2020. 2020, p. 8, NBC.
- [84] ÖNORM B 1991-1-4:2023-04.
- [85] DIN EN 1991-1-4.
- [86] DIN EN 1991-1-3.
- [87] SFS EN 1991-1-4.
- [88] SFS EN 1991-1-3.